

Special Collection:

Dust and dust storms: From physical processes to human health, safety, and welfare

Key Points:

- Wind-deposited light-absorbing particles (LAPs) on snow surfaces in the Colorado Rockies diminished laboratory-measured spectral reflectance
- Carbon-rich matter and dark rock particles indicated by magnetite abundance were most responsible for the diminished reflectance
- Interannual (2013–2016) variations were caused by variable amounts of LAPs from many natural and anthropogenic sources

Supporting Information:

Supporting Information may be found in the online version of this article.

Correspondence to:

R. L. Reynolds and H. L. Goldstein,
rreynolds@usgs.gov;
hgoldstein@usgs.gov

Citation:

Reynolds, R. L., Goldstein, H. L., Kokaly, R., Lowers, H., Breit, G. N., Moskowicz, B. M., et al. (2025). Light absorbing particles deposited to snow cover across the Upper Colorado River basin, Colorado, 2013–2016: Interannual variations from multiple natural and anthropogenic sources. *Journal of Geophysical Research: Atmospheres*, 130, e2024JD041676. <https://doi.org/10.1029/2024JD041676>

Received 24 MAY 2024

Accepted 9 JAN 2025

Published 2025. This article is a U.S. Government work and is in the public domain in the USA. *Journal of Geophysical Research: Atmospheres* published by Wiley Periodicals LLC on behalf of American Geophysical Union. This is an open access article under the terms of the [Creative Commons Attribution-NonCommercial-NoDerivs License](https://creativecommons.org/licenses/by/4.0/), which permits use and distribution in any medium, provided the original work is properly cited, the use is non-commercial and no modifications or adaptations are made.

Light Absorbing Particles Deposited to Snow Cover Across the Upper Colorado River Basin, Colorado, 2013–2016: Interannual Variations From Multiple Natural and Anthropogenic Sources

Richard L. Reynolds^{1,2} , Harland L. Goldstein¹, Raymond Kokaly³, Heather Lowers³ , George N. Breit³ , Bruce M. Moskowicz² , Peat Solheid², Jeff Derry⁴, and Corey R. Lawrence¹ 

¹U.S. Geological Survey, Geosciences and Environmental Change Science Center, Denver, CO, USA, ²Institute for Rock Magnetism, Department of Earth and Environmental Sciences, University of Minnesota, Minneapolis, MN, USA, ³U.S. Geological Survey, Geology, Geophysics, Geochemistry Science Center, Denver, CO, USA, ⁴Center for Snow and Avalanche Studies, Silverton, CO, USA

Abstract Atmospheric particulate matter (PM) as light-absorbing particles (LAPs) deposited to snow cover can result in early onset and rapid snow melting, challenging management of downstream water resources. We identified LAPs in 38 snow samples (water years 2013–2016) from the mountainous Upper Colorado River basin by comparing among laboratory-measured spectral reflectance, chemical, physical, and magnetic properties. Dust sample reflectance, averaged over the wavelength range of 0.35–2.50 μm , varied by a factor of 1.9 (range, 0.2300–0.4444) and was suppressed mainly by three components: (a) carbonaceous matter measured as total organic carbon (1.6–22.5 wt. %) including inferred black carbon, natural organic matter, and carbon-based synthetic, black road-tire-wear particles, (b) dark rock and mineral particles, indicated by amounts of magnetite (0.11–0.37 wt. %) as their proxy, and (c) ferric oxide minerals identified by reflectance spectroscopy and magnetic properties. Fundamental compositional differences were associated with different iron oxide groups defined by dominant hematite, goethite, or magnetite. These differences in iron oxide mineralogy are attributed to temporally varying source-area contributions implying strong interannual changes in regional source behavior, dust-storm frequency, and (or) transport tracks. Observations of dust-storm activity in the western U.S. and particle-size averages for all samples (median, 25 μm) indicated that regional dust from deserts dominated mineral-dust masses. Fugitive contaminants, nevertheless, contributed important amounts of LAPs from many types of anthropogenic sources.

Plain Language Summary Melting snow and ice on temperate-zone mountains provide critical water sources for downstream communities and ecosystems. An important factor contributing to the onset and rate of snow and ice melt is atmospherically deposited mineral dust and carbon-rich particles that darken snow and ice surfaces thereby absorbing light and emitting heat. Mineralogic, chemical, and physical property investigations of particulate matter (PM) on snow surfaces of the Colorado Rocky Mountains (collected 2013–2016) revealed three classes of heat-absorbing particles: (a) dark carbonaceous matter, (b) dark rock and mineral particles, and (c) very small iron oxide minerals. The many sources of the carbon-rich particles include (a) fossil-fuel and wood combustion, such as soot, (b) black microplastics from worn road tires, and (c) plant matter, including pollen. The types and amounts of rock-derived particles varied greatly from year-to-year partly reflecting variable contributions from different dust-source regions perhaps caused by varying landscape conditions in source regions and (or) dust-transport pathways. Models describing the influence of PM on snowmelt in the Colorado Rockies might benefit from accounting for year-to-year variations in the amounts and compositions of light-absorbing particulate matter.

1. Introduction

The timing and rate of temperate zone ice and snowmelt strongly influence the health of downstream, water-dependent ecosystems, and human communities (Viviroli et al., 2007). In addition to air temperature, the amounts and types of light-absorbing particulate (LAP) matter deposited from the atmosphere are important controls, by emitting heat, on snow and ice melt (Di Mauro et al., 2019; Painter et al., 2012a, 2012b). An additional control is snow metamorphism producing rough surface textures.

An important class of LAPs comprises carbonaceous, non-mineral matter (including black carbon, BC), having numerous origins (e.g., Bond & Bergstrom, 2006; Bond et al., 2013; Flanner et al., 2007, 2009, 2012). Many studies have examined the combined effects of BC, specifically, and mineral dust, generally, on snow cover albedo and related snow melt (e.g., Dang et al., 2017; Doherty et al., 2013; Dumont et al., 2020; Gleason et al., 2022; Hadley et al., 2010; He, 2022; He et al., 2019; ; Kaspari et al., 2014, 2015; Nagorski et al., 2019; Oaida et al., 2015; Rahimi et al., 2020; Sarangi et al., 2020; Skiles et al., 2018; Skiles & Painter, 2018; Wang et al., 2013; Wu et al., 2018; Yasunari et al., 2014; Y. Zhang, Goldstein, et al., 2018; Zhao et al., 2014; Zhong et al., 2021). Relatively few, however, have systematically evaluated specific dust minerals for their effects on snow melt (e.g., Axson et al., 2016; Di Mauro et al., 2019; Kaspari et al., 2014), examples of which are dark rock (e.g., basalt) and mineral (e.g., magnetite) particles having strong heat-absorbing properties (Clark, 1983; Kokaly et al., 2017; Reynolds, Goldstein, et al., 2014, 2020). Another class of dust-mineral LAPs comprises the ferric oxide minerals: hematite and goethite (Alfaro et al., 2004; Derimian et al., 2008; Englebrecht et al., 2016; Lafon et al., 2004, 2006; Moosmüller et al., 2012; Sokolik et al., 2001; Zhang et al., 2015). Further, particles of microplastics (defined as plastics less than 5 mm in any dimension) comprise a recently recognized class of carbon-based LAP matter on cryogenic surfaces (e.g., Allen et al., 2019, 2022; Bergmann et al., 2019; Brahney et al., 2020, 2021; Evangelidou et al., 2020; Ming & Wang, 2021). Examination of dry- and (or) wet-deposition samples has revealed the occurrences of microplastics in many remote locations in the American West (Brahney et al., 2020; Wetherbee et al., 2019).

Recent research has demonstrated the deleterious effects of air-deposited particulate matter (PM) on the timing and rate of snowmelt in the Upper Colorado River basin, and the challenges that these effects have on water-resource management throughout the region (Deems et al., 2013; Landry et al., 2014; Naple et al., 2024; Painter et al., 2007, 2010, 2012a, 2012b, 2018, 2018; Skiles et al., 2012, 2015, 2017; Skiles & Painter, 2016, 2017; Udall, 2013). Relative to pre-European settlement (about 1860 CE), a combination of measurements and modeling points to direct effects of dust loading on the reduction of snow cover and the onset of snow melt by 25–51 days (Painter et al., 2007, 2010, 2018; Skiles et al., 2012). All such melting puts water into downstream storage earlier than is desirable because early, heavy pulses of runoff sometimes must be quickly passed through storage reservoirs. Under these conditions, total available water supply is lessened during the hottest and driest parts of summer when water is most needed. Seasonal snow in the Colorado River basin provides most of the water for heavily populated drylands (about 44 million inhabitants) of the American Southwest and parts of Mexico through which the Colorado River flows.

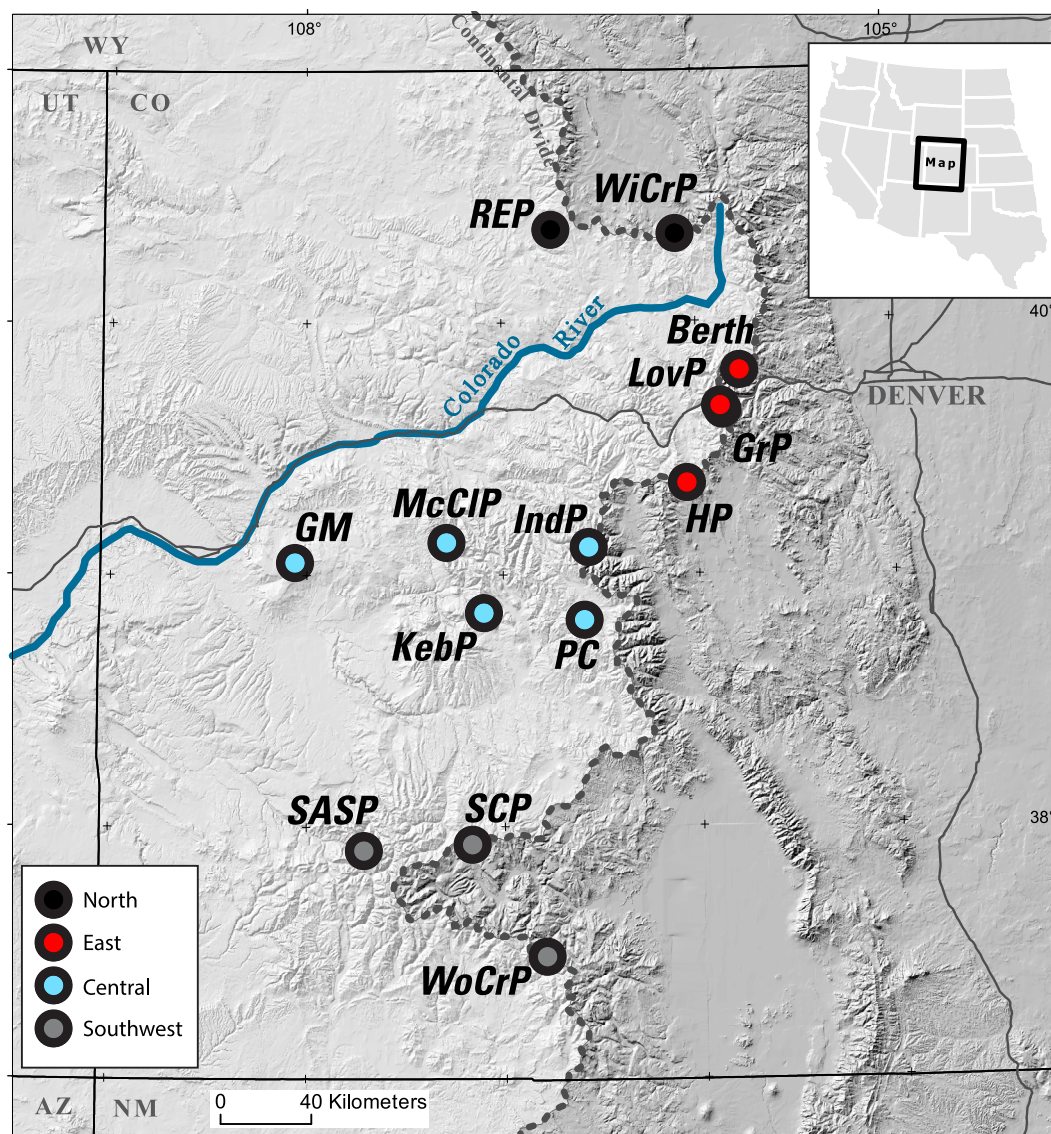
Major foci of this study were (a) to identify LAPs in snow within much of the UCRB by evaluating interrelations among laboratory-measured spectral reflectance, mineralogic, textural, and chemical properties, (b) to determine variations in LAP amounts over time and space, and (c) to assess causes for their variations. The data on LAPs and their effects on spectral reflectance, after further translation to albedo (not done here), can be applied to snow hydrologic modeling when evaluating interannual changes in water-resource availability within this large catchment.

2. Samples and Methods

2.1. Sample Collection and Preparation

Samples of dust-laden snow surfaces were collected at repeat study sites during ongoing studies of snow hydrologic conditions across part of the UCRB (Figure 1; Table 1). The samples, from 14 sites distributed across an area of about 60,000 km², were collected over four years from water year 2013 (WY13) through WY16. For example, WY16 began 1 October 2015 and ended 30 September 2016. Collections were made late during the melt season attempting to capture the last remaining layer of dust—the All Layers Merged (ALM) samples—after individual, previously wind-deposited dust layers had coalesced at the snow surface. Several times, snow had melted completely before sampling was possible, so that some sites lacked an ALM sample for a given water year (Table 1). In all, 38 samples were taken, including four from the Swamp Angel Study Plot (SASP) site for which results were previously described (Reynolds et al., 2020) and are reported herein for completeness. Site settings and underlying geologic substrates are listed in Table S1 in Supporting Information S1.

Samples were collected by scraping the top 2–5 cm of the dust-laden snow surface with an aluminum shovel. The ALM samples were taken to maximize amounts of PM; thus, sample mass did not indicate dust flux. The samples were placed in plastic carboys and shipped to U.S. Geological Survey laboratories in Denver, Colorado where



Shaded relief created from National Elevation Dataset(NED)

Figure 1. Map showing locations of sampling sites within the UCRB. Abbreviations explained in Table 1. Marker colors indicate groups by location: gray, southwest; cyan, central; red, east; black, north. Dashed line denotes the Continental Divide. Latitudes, north; longitudes, west.

water from melted snow with dust was evaporated at 45-degrees C. Visible fragments of plant matter, such as conifer needles, were removed by hand. Each dried sample was divided so that all measurements were made on splits from the same sample.

2.2. Reflectance

Reflectance spectra were measured on dried samples in aluminum cups using an Analytical Spectral Devices (ASD) Inc. FieldSpec3 spectrometer, covering the wavelength range of 0.35–2.50 μm in 2,151 channels. The spectrometer is calibrated for wavelength position and radiance by the manufacturer on an annual basis. Spectral reflectance was measured relative to a Labsphere Spectralon® 99% reflectance reference panel. The average reflectance spectrum for each sample was converted to absolute reflectance, adjusting for the absorption properties of the reference panel (Kokaly & Skidmore, 2015). Reflectance measurements of bulk samples were expressed as the averages over (a) the total solar energy spectrum (0.35–2.50 μm ; R_{tot}) and (b) the visible portion of the spectrum (0.4–0.7 μm ; R_{vis}). Sources of uncertainty include the measurement protocol and instrumentation

Table 1
Sites and Their Locations (Latitudes, North; Longitudes, West), Site Abbreviations in Figure 1, and Water Years (WY) of Collection

Site	Abbrv.	Latitude	Longitude	Elevation (m)	Location	WY
Berthoud Pass	Berth	39.8033	−105.7776	3,444	East	13–16
Grand Mesa	GM	39.0508	−108.0613	3,240	Central	13–16
Grizzly Peak	GrP	39.6471	−105.8689	3,383	East	13,14,16
Hoosier Pass	HP	39.3590	−106.0582	3,474	East	13,14,16
Independence Pass	IndP	39.1081	−106.5644	3,690	Central	14
Kebler Pass	KebP	38.84976	−107.1003	3,058	Central	15
Loveland Pass	LovP	39.66337	−105.8791	3,658	East	15
McClure Pass	McCIP	39.1294	−107.2885	2,896	Central	13,14,16
Park Cone	PC	38.8194	−106.5902	2,926	Central	13,14,16
Rabbit Ears Pass	REP	40.3683	−106.7388	2,865	North	13,14
Swamp Angel Study Plot	SASP	37.9069	−107.7114	3,371	Southwest	13–16
Spring Creek Pass	SCP	37.9304	−107.1653	3,292	Southwest	13,14,16
Willow Creek Pass	WiCrP	40.3481	−106.0953	2,908	North	13,14
Wolf Creek Pass	WoCrP	37.4838	−106.7955	3,336	Southwest	13–16

(sample loading, illumination, and spectrometer stability). To assess the uncertainty related to the measurement protocol, nine measurements of an internal standard were made across five measurement sessions (August 2014 to July 2016). The mean R_{tot} for the internal standard was 0.5230 (standard deviation = 0.0083). The largest uncertainty (95% confidence interval) for the Spectralon panel reflectance propagated to a 0.0127 uncertainty in reflectance for the internal standard. Ferric oxide minerals were identified by analyzing reflectance spectra using the Material Identification and Characterization Algorithm (MICA), a module of the PRISM software system (Kokaly, 2011), which uses continuum removal to isolate diagnostic absorption features and linear regression to compare spectral features. In this way, the spectra of the samples were compared with reference spectra of minerals and other materials (Kokaly et al., 2017). The MICA analysis computes a fit value, ranging from 0 to 1, between the sample spectrum and each reference material (Kokaly, 2011), with “best fit” determined by the highest fit value.

2.3. Magnetic Properties and Iron Mineralogy

Magnetic measurements were made on bulk dried sediment packed into 3.2-cm³ plastic cubes and normalized for sample mass. Remanent magnetization was measured using a 90-Hz spinner magnetometer with a sensitivity of 10^{−5} Am^{−1}. As part of the initial setup for each batch of samples, a calibration sample was run, and then the empty spinner as well as an empty cube holder were measured. A measure of the quantity of magnetite sufficiently large (magnetic grain size greater than about 30 nm) to carry remanence is referred to as isothermal remanent magnetization (IRM_{0.3T}), the magnetization acquired by a sample after exposure to a 0.3-T (T) magnetic field. Hard IRM (hard isothermal remanent magnetization (HIRM)), a measure of high-coercivity ferric oxide minerals (hematite and goethite), is calculated (IRM_{1.2T}−IRM_{0.3T})/2. A measure of magnetic grain size for magnetite is the ratio of anhysteretic remanent magnetization (ARM) to IRM_{0.3T} (ARM/IRM). Magnetic grain size, which may not indicate the physical size of a magnetite particle, reflects the magnetic domain structure of magnetic minerals, thereby providing information about origins of these minerals. The values of ARM/IRM increase with decrease in magnetic grain size, and it is particularly sensitive to single domain and small pseudo-single domain (PSD) sizes (~30–1,000 nm). Anhysteretic remanent magnetization was imparted in a DC induction of 0.1 mT in the presence of a decaying alternating induction from 100 to 0 mT. Magnetic susceptibility (X) was determined in a 0.1 mT induction at 600 Hz using a susceptometer with a sensitivity better than 4 × 10^{−7} m³ kg^{−1}. A subset of 20 samples was analyzed for saturation magnetization (M_s) using a vibrating magnetometer (VSM, Lake Shore model 8,600). Weight percent magnetite was determined as sample $M_s/92$ Am² kg^{−1} × 100. Types of iron minerals and their hosts were observed in bulk samples using a stereomicroscope and in polished grain mounts of magnetic grains using a petrographic microscope at 400x under reflected light.

2.4. Carbonaceous Matter

Carbon content was measured with an Elementar Soli total organic carbon (TOC) Cube (Elementar Analysensysteme GmbH, Langensfeld, Germany) under a gas-switching method with temperature-dependent-oxidation. Dried samples were weighed in ceramic crucibles and loaded into the instrument autosampler. During the measurement of each sample, the temperature of the combustion oven was first ramped to 400°C in an oxygen environment, and the resulting CO₂ was measured on the Soli TOC Cube near-infrared detector. The carbon oxidized and measured in this step is considered organic carbon (OC₄₀₀). Next, the carrier gas was switched from oxygen to nitrogen and the oven temperature ramped to 900°C. The resulting CO₂ corresponded to total inorganic carbon (TIC). As a last step, the carrier gas was switched back to oxygen with the oven remaining at 900°C, and any remaining carbon—the residual oxidizable carbon (ROC)—was converted to CO₂ and measured. With this method, the total carbon (TC) content of the sample is the sum of the three carbon components measured (TC = OC₄₀₀ + TIC + ROC). The total organic carbon (TOC) content of the sample is the sum of OC₄₀₀ and ROC (TOC = OC₄₀₀ + ROC). Total organic carbon was measured on solid-phase samples. Dissolved organic carbon was not measured, as any dissolved carbon is retained in the solid-phase after evaporation. Quality protocol included running a suite of control samples following every 10 unknowns. Control samples consisted of blanks, known standards (accuracy), and duplicated unknowns (precision). Based on these control samples, our analyses were accurate to within 0.1% of the accepted values (TC ± 0.08%, TOC ± 0.08%, and TIC ± 0.02%), and the duplicate precision was <±3% with both metrics reflecting relative deviation not absolute concentrations. Unknown sample concentrations were corrected for laboratory blanks by subtracting the mean blank peak area (CO₂) from each sample peak area prior to calculating sample concentrations. The mean peak area of sample blanks was less than 0.01% of mean sample peak areas. Values of magnetic properties and elemental amounts were recalculated from initial values on an organic-matter free basis to correct for the dilution of bulk dust by organic matter estimated by multiplying TOC wt % by the standard factor of 1.72. This necessary adjustment introduced some unknown degree of uncertainty because not all TOC contained the same amounts of non-carbon elements represented in the standard factor.

2.5. Major and Trace Elemental Chemistry

Elemental amounts were determined following four acid digestion (a mixture of hydrochloric, nitric, perchloric, and hydrofluoric acids) by analyzing the resulting solution by inductively coupled plasma—atomic emissions spectrometry (ICP-AES) for Al, Fe, Ca, K, Mg, Na, P, Ti, Mn, and Nd using measurement protocols of standards and blanks by Briggs (2002) and inductively coupled plasma—mass spectrometry (ICP-MS) for the other reported elements using measurement protocols of standards and blanks by Briggs and Meier (2002) and Wolf and Adams (2015).

2.6. Microscopy

Observations of samples were made under a Keyence VX-7000 stereomicroscope at 80–700x and a scanning electron microscope (SEM; FEI Quanta 450 FEG) equipped with an energy-dispersive spectrometer (EDS; Oxford Instruments XMax^N 50). Operating conditions for secondary and backscatter-electron imaging and EDS collection were variable depending on the particle but resulted in imaging resolutions of 50 nm and enabled detection of elements from 0.2 to 9 KeV (C to Zn K α). Samples were prepared for SEM-EDS examination by placing hand-picked particles on adhesive SEM-stub surfaces that were then lightly coated with carbon prior to examination.

2.7. Particle-Size Analysis

Particle sizes between 0.06 and 2,000 μ m were measured using laser-diffraction methods (Malvern Mastersizer 2000) and reported as volume percent. Prior to analysis, samples were prepared by digestion in 30% H₂O₂ to remove organic matter and deflocculated in a Na-hexametaphosphate solution.

3. Results

The results are considered by iron oxide mineralogy, water year, and site location as primary variables to assess the causes of variations in reflectance. For locations, the sampling sites were divided into four geographic sectors

as indicated in Figure 1 and Table 1: southwest, central, east, and north. These designations were drawn before examining data and remained unchanged.

3.1. Reflectance

Total reflectance (R_{tot}) of the ALM samples averaged 0.3574 (standard deviation (sd), 0.0548) and varied by a factor of 1.9 (range, 0.2300–0.4444); visible reflectance (R_{vis}) averaged 0.1755 (sd, 0.0246) and varied by a factor of 1.6 (range, 0.1297–0.2082) (Table 2). Total reflectance varied significantly for the WY13 versus WYs 14, 15, and 16 samples ($P < 0.001$) as well as for WY15 versus WY16 ($P = 0.011$; one-way ANOVA, Holm-Sidak-test pair-wise comparisons). Highest average R_{tot} values were for WY13 (0.4191) and lowest for WY 15 (0.2851) (Figure 2; Table 2). The highest average R_{vis}, also for WY13, was 0.1988, and lowest R_{vis} average values were 0.1578 (WY14) and 0.1604 (WY15).

Overall, R_{tot} and R_{vis} values lacked tight correspondence ($r^2 = 0.57$; Figure 3), and four clusters represented the four WY sets: The WY15- and 16-sample values defined two partly overlapping trends, WY14 values defined a different but nearly parallel trend, and WY13 values clumped in a field of relatively high R_{tot} and R_{vis}. The data fields and trends revealed interannual variations caused by fundamentally different compositions of PM as amplified in the following. Reflectance values varied without significant differences among the four regions.

3.2. Iron Oxide Mineralogy

Each sample contained ferric oxide minerals and magnetite on the combined basis of reflectance spectroscopy, magnetic properties, and microscopy. The samples were divided into three iron-oxide mineral groups—goethite, hematite, and magnetite (Table 2). The goethite and hematite groups were discerned on the sole presence or dominance of either mineral identified in reflectance spectra. The goethite group consisted of 21 samples of which seven contained lesser hematite, and the hematite group consisted of 10 samples of which eight contained lesser goethite. Thus, goethite and hematite were noted together in 15 of the 31 samples having spectrally identifiable Fe oxide. The magnetite group comprised seven samples, spectrally indeterminate for ferric oxide mineral, without a priori regard for magnetite abundance in them.

Samples of the three mineral groups were distributed unevenly across time and space (Figure 4). Goethite dominated in all WY13 and in most WY15 samples. Hematite dominated in the WY14 samples albeit with goethite as secondary in most. The magnetite-group samples made up the majority of WY16 samples. By location, goethite was present in all geographic groups, dominating in the southwest group, whereas hematite prevailed in the central group. Most magnetite-group samples appeared in the east group and none in the north group.

Coincidentally, the magnetite-group samples had significantly higher amounts of magnetite ($P < 0.001$ on median values) on the basis of IRM and magnetic susceptibility compared with ferric oxide-group samples (Figure 5). In the subset of 20 samples measured for *M_s*, magnetite ranged 0.11–0.37 wt. % (mean = 0.26 wt. %) in the six magnetite-group samples and 0.05–0.29 wt. % (mean = 0.12 wt. %) in the others (Table 2). By location, respective IRM and HIRM magnitudes mostly overlapped. The values of ARM/IRM were significantly lower ($P < 0.05$) for the magnetite-group samples compared to the identical values for the goethite and hematite groups, indicating the presence of larger magnetic grain size (reflecting magnetic domain state) in these relatively magnetite-rich samples (Figure 5).

Considering all samples, IRM roughly corresponded with HIRM ($r^2 = 0.39$), as expected because of the close genetic associations between ferric oxide and magnetite in many types of igneous rocks and sediments derived from them. The IRM-HIRM relations, however, were distinct among the hematite, goethite, and magnetite groups. In the hematite group, ferric oxide (HIRM) corresponded with magnetite (IRM, $r^2 = 0.87$) much more tightly than in the goethite-group ($r^2 = 0.55$) and with steeper slope (Figure 6).

3.3. Carbonaceous Matter

Total organic carbon ranged 1.61–22.48 wt. % (mean, 7.80 wt. %, sd, 5.81 wt. %; Table 2; Table S2 in Supporting Information S1). The magnetite-group samples together possessed more TOC than did the goethite- and hematite-group samples (Figure 7a). By water year, TOC amounts were relatively low in the WY13 and WY14 samples and

Table 2
List of Samples by Site, Year of Collection, and Location With Associated Properties

Site	WY	LOC	FeOx1	FeOx2	Rtot	Rvis	TOC wt%	Magnetite wt%	Xlf	IRM	HIRM	ARM/IRM	JD
Berthoud Pass	13	E	Gt		0.44441	0.20646	1.97		5.4E-07	6.2E-03	4.5E-04	0.026	141
Grand Mesa	13	C	Gt	Ht	0.41155	0.20745	4.02	0.10	8.0E-07	1.0E-02	6.5E-04	0.022	141
Grizzly Peak	13	E	Gt		0.40206	0.20484	3.00	0.14	9.0E-07	9.9E-03	4.7E-04	0.022	141
Hoosier Pass	13	E	Gt		0.39715	0.17905	2.27		1.2E-06	1.4E-02	5.4E-04	0.023	142
McClure Pass	13	C	Gt		0.41026	0.20563	10.91	0.12	8.7E-07	1.1E-02	6.8E-04	0.019	120
Park Cone	13	C	Gt		0.40438	0.19613	5.81		6.6E-07	7.9E-03	4.0E-04	0.021	120
Rabbit Ears Pass	13	N	Gt	Ht	0.39759	0.17952	2.55	0.10	8.0E-07	1.0E-02	7.3E-04	0.026	131
SASP	13	SW	Gt		0.44188	0.20668	1.87	0.05	5.2E-07	6.1E-03	4.5E-04	0.020	133
Spring Creek Pass	13	SW	Gt	Ht	0.42820	0.20138	3.14		5.6E-07	6.9E-03	5.4E-04	0.018	121
Willow Creek Pass	13	N	Gt	Ht	0.44061	0.20287	2.51		5.4E-07	7.2E-03	7.6E-04	0.031	130
Wolf Creek Pass	13	SW	Gt		0.43255	0.19649	3.21		7.7E-07	9.4E-03	1.6E-04	0.017	121
Berthoud Pass	14	E	Gt	Ht	0.32448	0.14412	6.29		8.4E-07	1.2E-02	7.4E-04	0.016	154
Grand Mesa	14	C	Ht	Gt	0.31104	0.13194	4.16	0.06	4.6E-07	6.6E-03	7.6E-04	0.020	153
Grizzly Peak	14	E	Gt	Ht	0.33662	0.16092	4.31		7.4E-07	6.6E-03	3.2E-04	0.013	154
Hoosier Pass	14	E	Ht	Gt	0.38948	0.18039	4.06		3.3E-07	3.9E-03	3.9E-04	0.019	154
Independence Pass	14	C	Ht	Gt	0.42968	0.18761	1.61	0.06	2.4E-07	3.0E-03	4.2E-04	0.022	153
McClure Pass	14	C	Ht	Gt	0.36006	0.15561	8.53		5.6E-07	7.2E-03	6.8E-04	0.020	116
Park Cone	14	C	Ht	Gt	0.34704	0.15127	4.01	0.06	2.0E-07	2.7E-03	3.3E-04	0.022	113
Rabbit Ears Pass	14	N	Gt		0.33873	0.16086	18.24		1.1E-06	1.5E-02	7.6E-04	0.019	155
SASP	14	SW	Ht	Gt	0.40685	0.17807	3.40		2.9E-07	6.5E-03	6.7E-04	0.019	148
Spring Creek Pass	14	SW	Ht	Gt	0.38172	0.15490	3.11		4.8E-07	7.0E-03	6.8E-04	0.020	114
Willow Creek Pass	14	N	Gt	Ht	0.30452	0.13324	5.37		5.1E-07	7.1E-03	6.8E-04	0.024	115
Wolf Creek Pass	14	SW	Gt		0.32822	0.15515	5.83		6.6E-07	9.3E-03	5.4E-04	0.022	137
Berthoud Pass	15	E	Mt		0.22998	0.12974	14.28	0.24	1.8E-06	2.3E-02	6.5E-04	0.013	166
Grand Mesa	15	C	Gt		0.27105	0.14618	16.63	0.14	1.0E-06	1.7E-02	9.1E-04	0.019	152
Kebler Pass	15	C	Gt		0.29238	0.16401	16.16	0.29	2.1E-06	2.9E-02	1.1E-03	0.017	152
Loveland Pass	15	E	Mt		0.29655	0.18478	8.25		1.9E-06	2.1E-02	5.9E-04	0.016	166
SASP	15	SW	Gt		0.30936	0.17342	11.04	0.17	1.3E-06	1.9E-02	1.0E-03	0.018	155
Wolf Creek Pass	15	SW	Gt		0.31104	0.16415	13.58	0.21	2.7E-06	3.7E-02	1.1E-03	0.014	152
Berthoud Pass	16	E	Mt		0.32818	0.19399	12.44	0.26	1.8E-06	2.3E-02	8.3E-04	0.017	153
Grand Mesa	16	C	Ht		0.37458	0.20149	8.52	0.10	6.9E-07	9.7E-03	7.9E-04	0.019	164
Grizzly Peak	16	E	Mt		0.35829	0.20819	5.50	0.37	2.6E-06	2.1E-02	5.3E-04	0.011	153
Hoosier Pass	16	E	Mt		0.31513	0.17510	9.15	0.26	1.9E-06	2.2E-02	8.6E-04	0.018	153
McClure Pass	16	C	Ht		0.33776	0.18492	20.50	0.14	1.0E-06	1.2E-02	9.4E-04	0.017	134
Park Cone	16	C	Mt		0.29409	0.15111	17.40	0.11	9.1E-07	1.2E-02	1.0E-03	0.020	134
SASP	16	SW	Gt		0.33969	0.18506	5.04		7.0E-07	9.4E-03	8.8E-04	0.021	164
Spring Creek Pass	16	SW	Ht	Gt	0.36671	0.19242	5.23		6.4E-07	8.2E-03	9.0E-04	0.021	134
Wolf Creek Pass	16	SW	Mt		0.28809	0.13289	22.48	0.33	2.2E-06	2.9E-02	1.1E-03	0.015	164

Note. Water year (WY) of collection; location group (LOC; E, east; C, central; N, north; SW, southwest). Fe Ox 1, dominant iron oxide mineral: ferric oxide (Gt = goethite, Ht = hematite) or magnetite (Mt) in the absence of ferric oxide identification. Fe Ox 2, subsidiary iron oxide from reflectance spectroscopy. Rtot, reflectance averaged over the total spectrum (0.35–2.5 μm); Rvis, reflectance averaged over the visible portion of a spectrum (0.4–0.7 μm). TOC, total organic carbon (wt. %); Magnetite (wt. %) from saturation magnetization, blank cells, not analyzed; Xlf, low-frequency magnetic susceptibility in m³ kg⁻¹; IRM, HIRM, and ARM (isothermal remanent magnetization, hard IRM, and anhysteretic RM, respectively) in Am² kg⁻¹. JD, Julian day of sample collection.

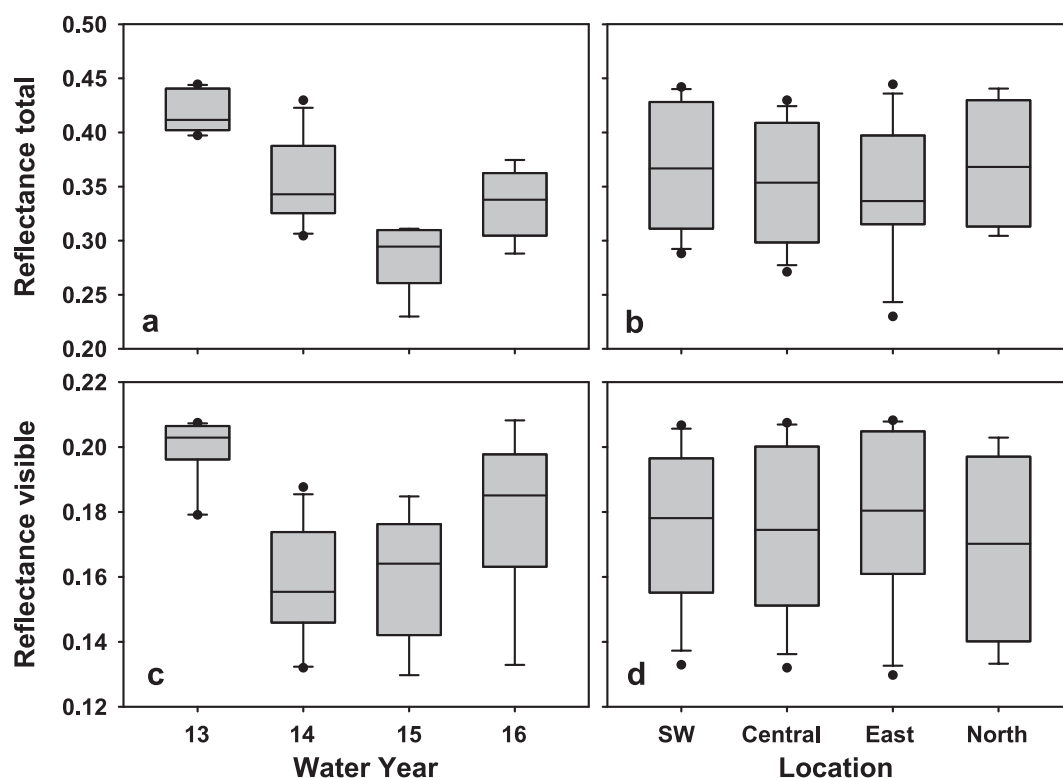


Figure 2. Box plots of average reflectance by water year and location over the total (a), (b) and visible (c), (d) parts of reflectance spectra. In this and following box plots, solid lines represent median values, the ends of the boxes define the 25th and 75th percentiles, and the error bars define the 10th and 90th percentiles. Dots indicate outliers.

high in the WY15 and 16 samples (Figure 7b). Among the location groups, TOC amounts varied greatly over the study period (Figure 7c).

As observed under stereomicroscopy and SEM-EDS, each sample contained numerous black particles of various shapes, sizes, metal composition, and textures (e.g., Figure S1 in Supporting Information S1). Some samples contained plant matter, including coniferous pollen, too small to have been removed by hand. Also found in each sample were fibers and fragments that by shape, size, and color were identical to particles described and illustrated

by others as microplastics (e.g., Allen et al., 2019; Bergmann et al., 2019; Brahney et al., 2020; Cowger et al., 2020; Dris et al., 2016; Hidalgo-Ruz et al., 2012; Wetherbee et al., 2019; Yang et al., 2023; Zambrano et al., 2019). Fibers, typically 10–100s μm in length and 5–10 μm in width, were variously colored (cloudy white/translucent, red/pink, green, blue, black, or banded in different colors). Twisted ribbons characterized the shapes of many fibers of all colors (see Xiao et al., 2023). Black PM was intimately associated with a few of the fibers either as thin (<10 μm -thick) coatings on fibers or within clusters of fibers, substances interpreted as road-tire-wear particles because identical particles have been found in road-surface samples and in shredded tires (Reynolds et al., 2024). Because of the possibility of contamination by white plastic particles—sample matter contacted white plastic during shipment and drying in the laboratory—we did not attempt to quantify the amount of microplastics.

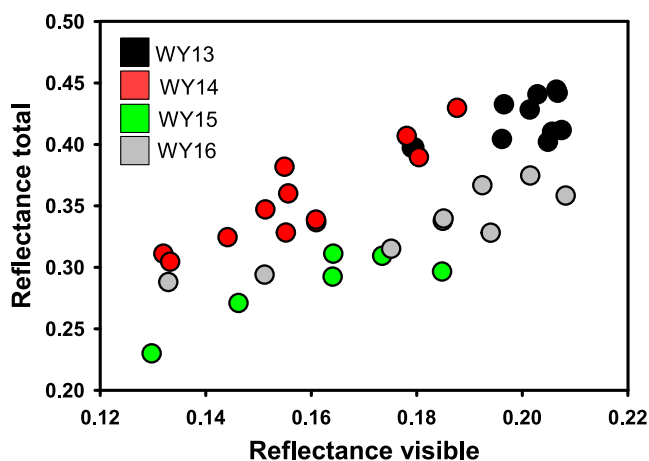


Figure 3. Plot of reflectance by water year; total, average over full spectrum (0.35–2.50 μm); visible, average over the visible portion of the spectrum (0.4–0.7 μm). Each marker represents a separate sample.

3.4. Major and Trace Element Chemistry

Most major elements exhibited some degree of mutual affinity (Tables S3 and S4 in Supporting Information S1). The correspondences of aluminum (Al)

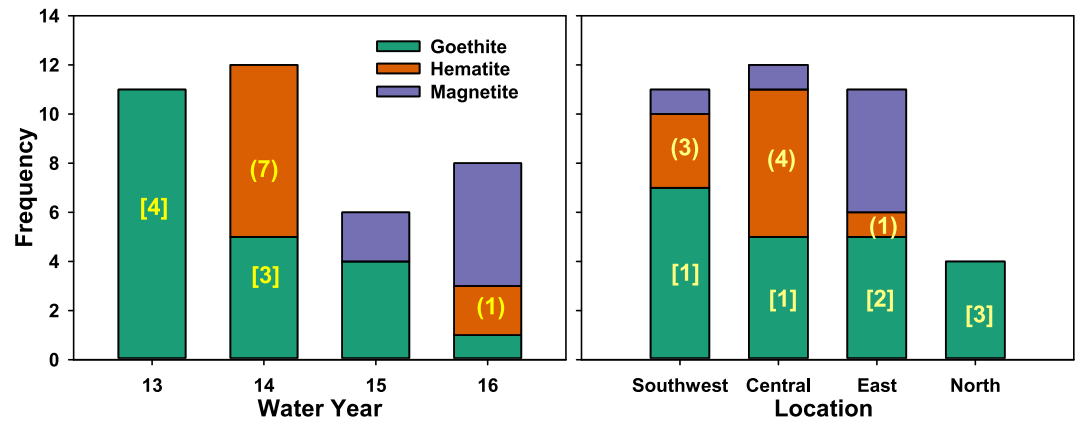


Figure 4. Number of samples (frequency) of iron oxide minerals on the basis of best-fit identifications from reflectance spectra and subdominant identifications (for hematite in brackets, goethite in parentheses) or magnetite in the absence of spectral identification of a dominant ferric oxide.

with iron (Fe), potassium (K), sodium (Na), and titanium (Ti) suggested their associations in common lithogenic dust minerals, such as clays and rock fragments. Calcium correlated only with Mg, but weakly so, in an expected association for Mg-bearing calcite and dolomite. Overall, most major-element amounts (Al, Fe, K, Na, Ti, and Mg) ranged by factors of 1.5–2.0 similar to factor ranges for R_{tot} and R_{vis} (Table S4 in Supporting Information S1).

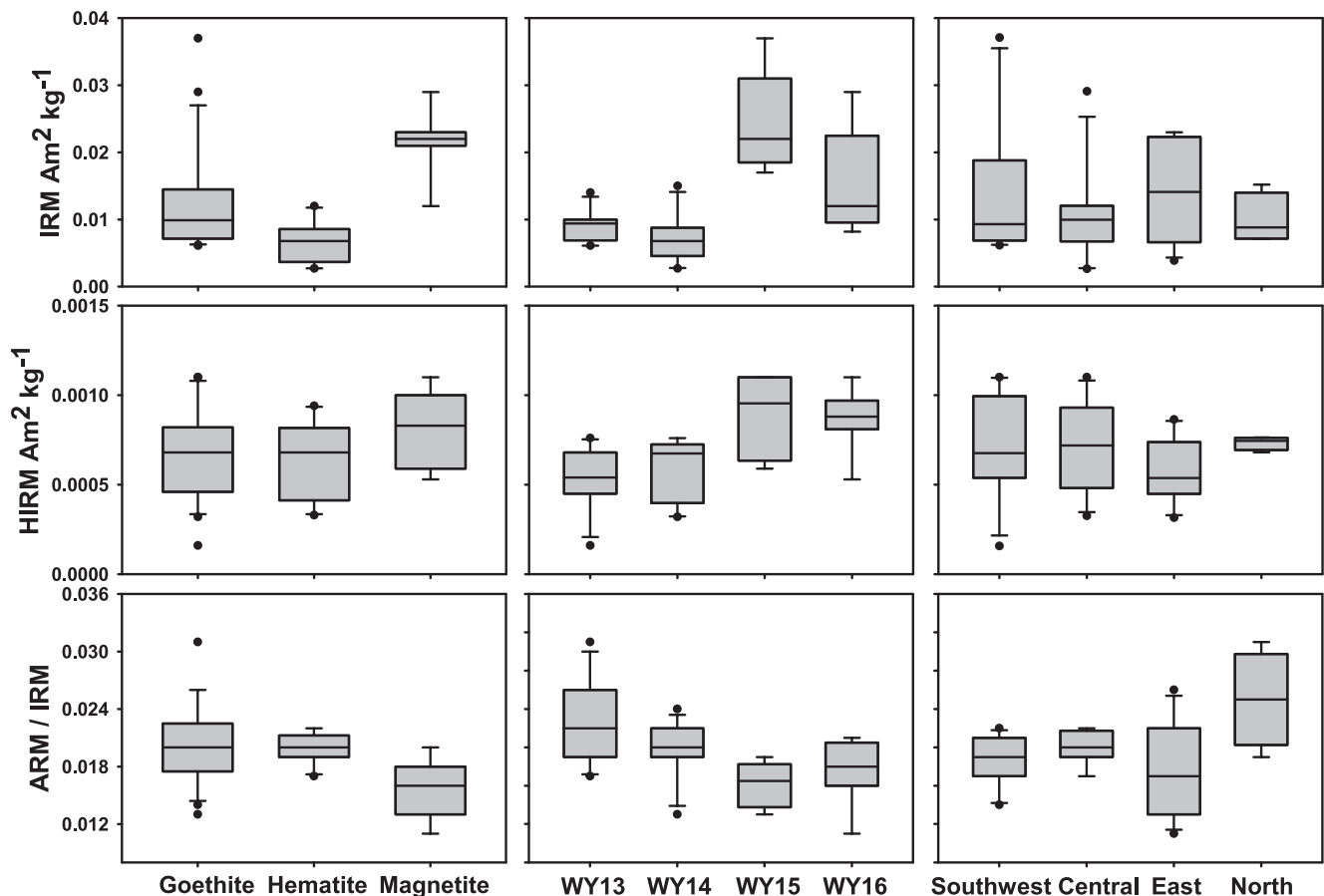


Figure 5. Box plots showing values of isothermal remanent magnetization (IRM), hard IRM (HIRM), and the anhysteretic remanent magnetization (ARM)/IRM ratio by groups; iron oxide (left panels), water years (WY, middle panels), and locations (right panels).

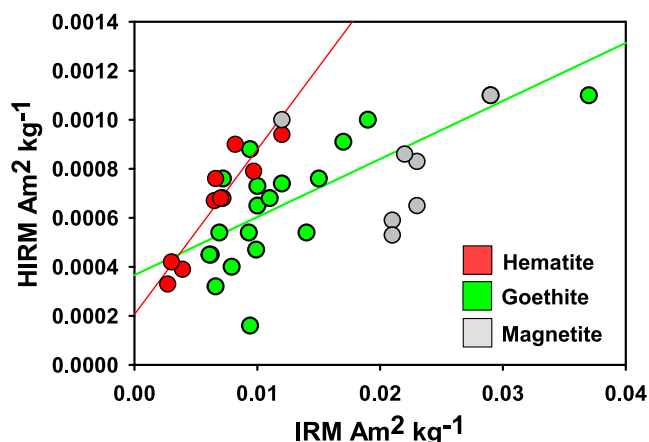


Figure 6. Plot of hard isothermal remanent magnetization (HIRM) versus IRM (overall $r^2 = 0.39$). Hematite-group samples obtained $r^2 = 0.87$; goethite-group samples, $r^2 = 0.55$. The magnetite samples lacked obvious correspondence in IRM and HIRM.

Only the average amounts of P and K, but barely, exceeded their respective average amounts for rocks of the upper continental crust (UCC; Rudnick & Gao, 2003; Table S5 in Supporting Information S1). The low relative amounts of most elements might have resulted from dilution by silica (not analyzed) especially in quartz in the weathered mature sedimentary rocks of the Colorado Plateau that provide numerous dust sources for UCRB dust (Reynolds et al., 2020).

Some major-element amounts differed within iron oxide mineral, water-year, and location groups. The magnetite-group samples possessed relatively high amounts of K, Na, P, Al, and Fe. Conspicuously low amounts of Al and Fe in the hematite-group samples were tightly correlated ($r^2 = 0.98$), whereas higher amounts of Al and Fe were less correlated in the goethite group ($r^2 = 0.29$) and the magnetite-group ($r^2 = 0.61$; Figure S2a in Supporting Information S1). Most major-element abundances varied greatly among water years, but Fe contents were an exception (Figure S3 in Supporting Information S1). Water-year-15 samples contained high amounts of Al, K, Na, and P; Na and P were also relatively abundant in WY16 samples. Calcium amounts were relatively high in WY13 and 14 samples possibly because of their early collection days as discussed in Section 4.2. Ranges in Ti amounts (not shown)

were similar across water years, locations, and iron-oxide groups. Large elemental variations typically existed within a location group thereby producing substantial overlap for a particular element among locations except for Fe, which separated into two groups: Low-iron amounts were characteristic of southwest and central sites compared with high iron in samples from the east and north sites. Aluminum amounts were relatively high in the east and north samples, such that a plot of Al versus Fe highlights the chemical differences between the southwest-plus-central group and the east-plus-north group (Figure S2b in Supporting Information S1).

Trace elements command attention because many of them hold clues to the origins of several LAPs (Carling et al., 2012, 2015; Clements et al., 2014; Dastrup et al., 2018; Goodman et al., 2019; Munroe et al., 2014; Reynolds, Goldstein, et al., 2014, 2020). Generally, wide ranging abundances of trace elements occurred in a variety of associations, some of them strongly correlated (Table S6 in Supporting Information S1). Average amounts of eight trace elements (Zn, As, Pb, Cu, Bi, Sb, Mo, and Cd in increasing order) were much larger than their respective average values in UCC rocks, average amounts of another 11 trace elements matched or were slightly greater than their respective UCC averages, and average amounts of nine were less than their respective UCC averages (Figure 8; Table S7 in Supporting Information S1).

The magnetite group possessed significantly greater amounts of nearly all trace elements relative to the goethite- and hematite-sample groups, with As, Cs, and Li as exceptions to this tendency (Figure 9 and S4). Goethite-group samples were enriched in trace elements compared with the hematite-group samples except for As, Cd, Li, Mn, Nd, and Y. The WY15 and most WY16 samples possessed relatively elevated trace-element amounts (Figure 9 and Figure S4 in Supporting Information S1).

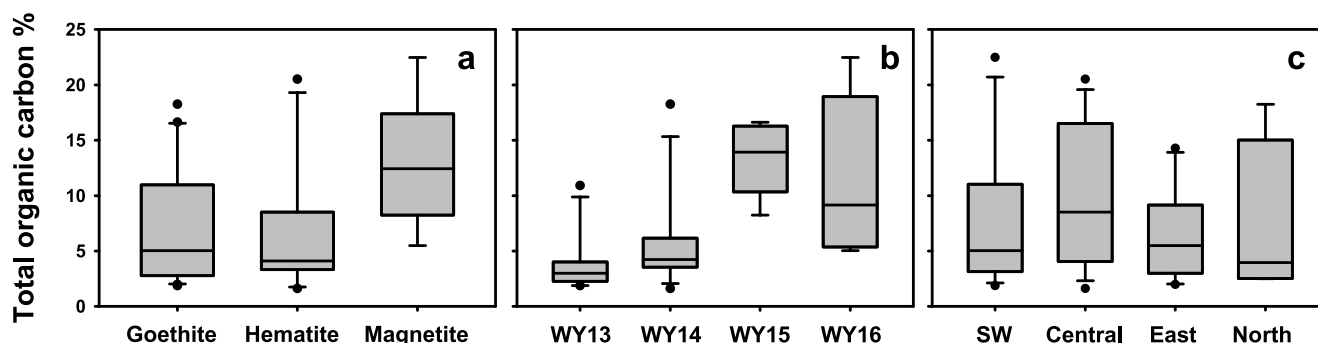


Figure 7. Total organic carbon in wt. % by (a) dominant iron oxide, (b) water year (WY), and (c) location.

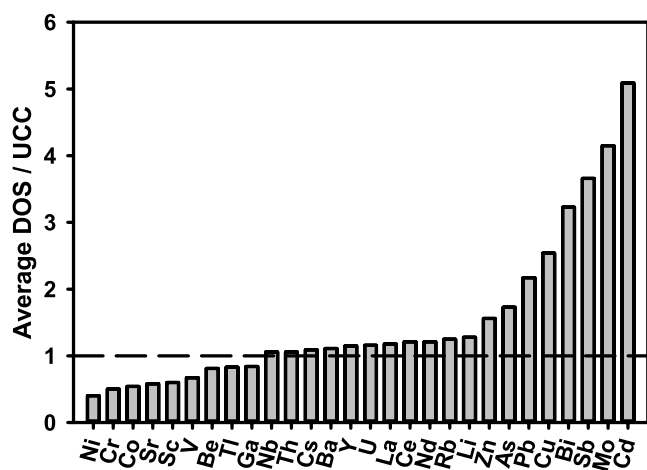


Figure 8. Bar plots of ratios of average trace elemental abundances in dust-on-snow (DOS; ALM matter) to respective Upper Continental Crust averages (UCC; Rudnick & Gao, 2003). Samples with anomalously high metal amounts were not used: Mo and Cu (106 and 215 ppm, respectively) in the WY16 Hoosier Pass sample; U, Th, and Y (71, 3,353, and 136 ppm, respectively) in the WY13 Grizzly Peak sample. Horizontal dashed line represents identical elemental abundances in ALM matter and UCC.

3.5. Particle-Size Distributions

Size distributions of PM overall indicated dominant silt (73.8 vol. %; sd, 4.6 vol. %) expressed similarly in PM_{63} (silt plus clay; mean, 85.7 vol. %; sd, 5.8 vol. %) and median size (mean, 24.8 μm ; sd, 5.6 μm) (Table S8 in Supporting Information S1). Amounts of $PM_{2.5}$, PM_{10} , PM_{20} , and sand averaged 8.2, 25.0, 43.0, 14.3 vol. %, respectively. Importantly, thus, the mean PM_{20-10} amount was 18% vol. %, and the mean PM_{63-10} amount was 60.7 vol. %. The iron oxide mineral groups exhibited some large differences in texture (Figure 10). The goethite-group samples had finest textures with respect to $PM_{2.5}$, PM_{10} , PM_{63} , sand, and median grain size, and the magnetite-group samples possessed relatively coarse texture in the silt, PM_{63} , and sand fractions. Nevertheless, hematite-group samples had the lowest average PM_{10} amounts (21% vol. %) and highest median grain size (29 μm).

Interannual variations in PSD parameters were small (Figure S5 in Supporting Information S1). The WY13 and 15 layers, however, were slightly enriched in PM_{10} and PM_{20} (not shown) roughly expressed also in relatively low median particle size (Table S8 in Supporting Information S1). These PSD-water year relations can be at least partly attributed to the dominance of relatively fine-grained goethite-group samples in the WY13 and 15 suites. There were no significant water-year differences within the $PM_{2.5}$ -size class. Among locations, the four north-site samples were relatively fine-grained especially

expressed as small median particle size (mean, 18.8 μm ; sd, 1.7 μm), high percentages of $PM_{2.5}$, PM_{10} , and PM_{63} as well as low percentages of sand (Figure S6 in Supporting Information S1). The east-group samples exhibited significantly highest amounts of sand along with correspondingly low amounts of silt and PM_{63} . Few associations existed among PSD parameters and trace elements, although relatively fine-grained textures expressed in median grain size (<27 μm) and $PM_{10-2.5}$ (>15% vol. %) but not $PM_{2.5}$ tended to contain relatively high amounts of Pb, Cu, As, Co, and Be (Figure S7 in Supporting Information S1).

4. Discussion

4.1. Relations Among Spectral, Mineralogic, Chemical, and Textural Properties

In the following, reflectance values are compared with iron oxide mineralogy, magnetic properties, chemical properties, and particle sizes. Relatively low R_{tot} characterized the magnetite-group samples compared with those of the goethite and hematite groups ($P = 0.009$ and 0.014 , respectively, one-way ANOVA, Holm-Sidak pairwise comparisons) for which R_{tot} values were statistically indistinct (Figure 11). The iron oxide groups had wide and similar ranges in R_{vis} . The observation that the magnetite-group samples yielded significantly lower values of R_{tot} but not of R_{vis} indicates that some components in these samples suppressed reflectance over the full solar-energy spectrum without prevalent effect on the visible portion.

Relatively low R_{tot} corresponded with relatively high IRM (magnetite amounts) and TOC ($r^2 = 0.37$ and $r^2 = 0.47$, respectively; Figure 12). In many samples, the effects of relatively high IRM and TOC apparently diminished R_{tot} to <0.36; nevertheless, other compositional factors must have contributed to such low R_{tot} (<0.36) in another six samples, which had relatively low IRM and TOC (Figure 13). Most samples having relatively low IRM and TOC possessed higher R_{tot} values. The crudely positive association between IRM and TOC is important with respect to particulate sources as amplified in Section 4.5.

Reflectance values showed no uniform correspondence with amounts of major elements except roughly for relatively high Al at low R_{tot} ($r^2 = 0.40$; Figure 14a). Aluminum amounts did not correspond with R_{vis} ($r^2 = 0.11$). Importantly, iron abundances did not influence R_{tot} ($r^2 = 0.07$; Figure 14b) or R_{vis} ($r^2 = 0.00$).

Values of R_{tot} corresponded with amounts of many trace elements. For example, high amounts of zinc corresponded with low R_{tot} and with relatively high TOC wt. % and IRM (Figure 15) as was found for Cu, As, Be, Y, Pb, and Nb. Regression fits of Zn were higher with IRM ($r^2 = 0.57$) than with TOC% ($r^2 = 0.41$). Overall, reflectance values lacked systematic dependence by any PSD parameter.

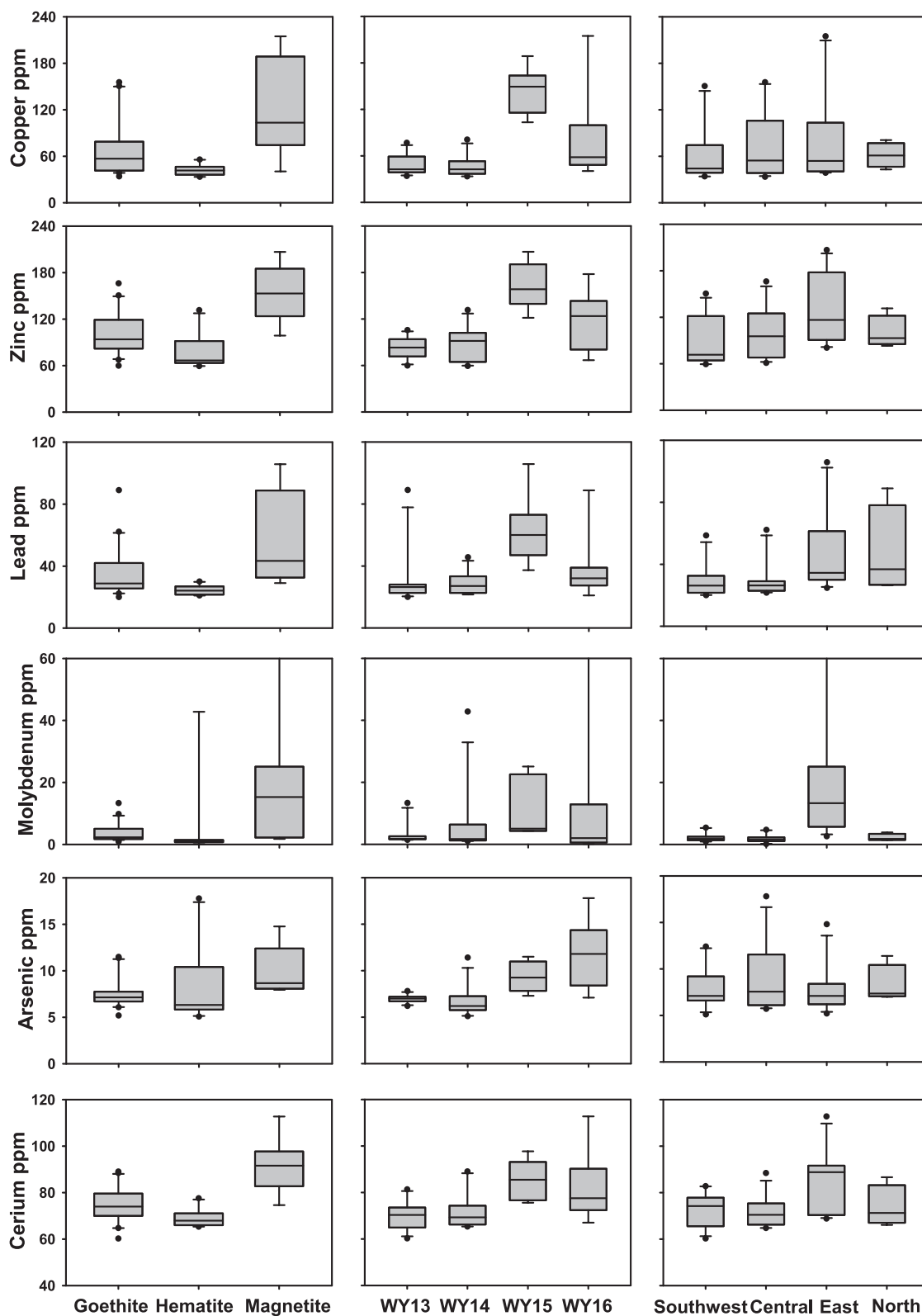


Figure 9. Box plots of trace-element amounts by groups: left column, iron oxide groups; middle column, water years (WY); right column, locations.

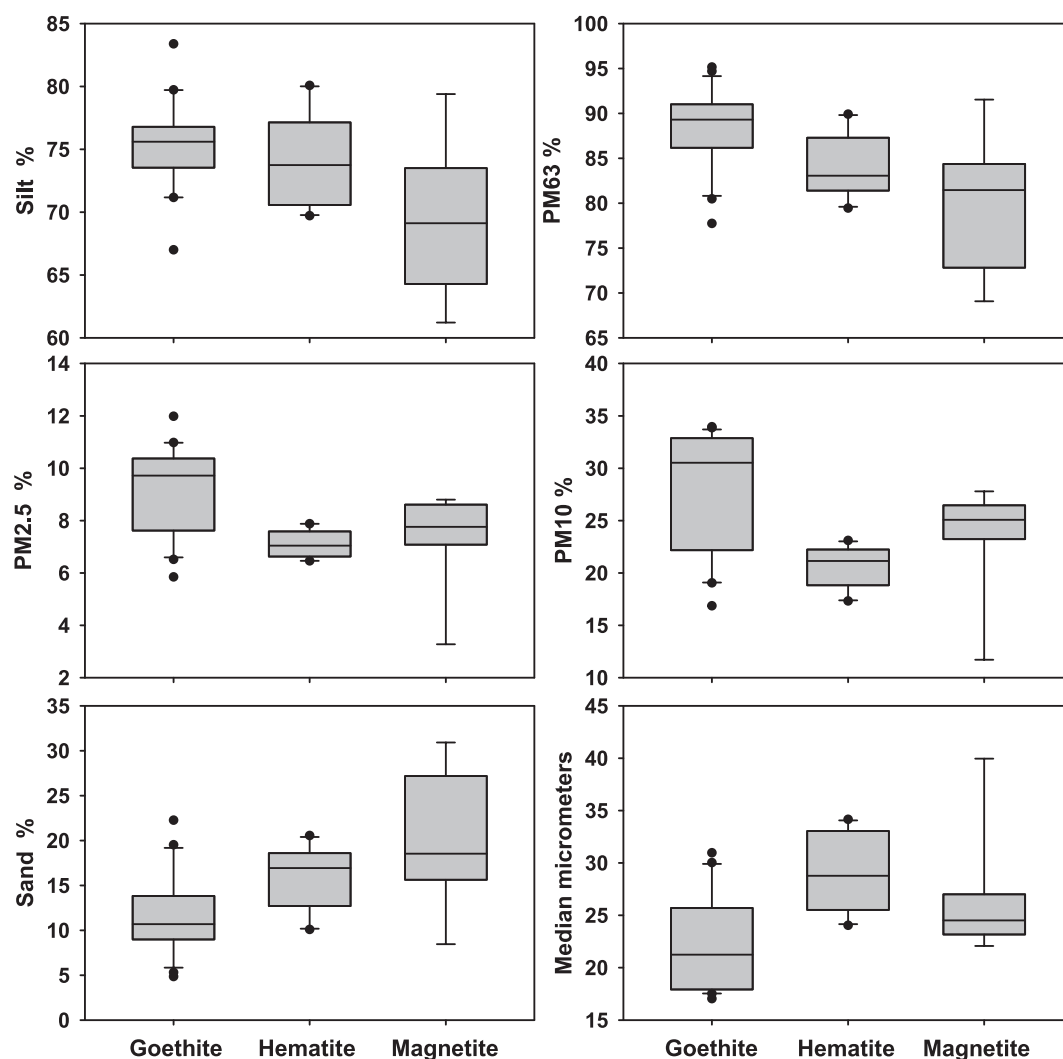


Figure 10. Box plots of particle-size parameters in vol. % and median size by iron oxide groups.

4.2. Influence of Collection Days on Physical and Chemical Properties

The timing of sample collection, counted by Julian days, influenced some properties. As examples, relatively late collection days of the WY15 samples corresponded roughly with relatively low R_{tot} , high IRM, high TOC wt. %, and with elevated trace elements as illustrated for Cu, Pb, Zn, Be, Ce, and Bi (Figures 16 and 17). These samples primarily came from the goethite- and magnetite-group samples as well as the WY15 and 16 samples. Similar dependence on collection day was indicated by the amounts of Ba, Ni, Nb, Mo, Sb, Sr, Rb, U, Th, and Tl (not shown).

4.3. Types and Occurrences of Light-Absorbing Particles

4.3.1. Carbonaceous Matter

Carbonaceous matter comprised several types having different origins each of which likely suppressed R_{tot} . The presence of BC as industrial/transportation pollutants is inferred by associations of TOC with metal (loids), including As, Ba, Be, Cd, Cu, Nb, Pb, Sb, Y, and Zn. That is, many samples with relatively high TOC (>7 wt.%) also possessed amounts of these trace elements greater than their average UCC amounts. In addition, pollen may have contributed as brown carbon to diminished average total reflectance in some samples. Black tire-wear microplastic particles likely contributed to diminished reflectance but by unknown degrees (Reynolds et al., 2024; Figure S1 in Supporting Information S1; see also Brahney et al., 2020; Evangelidou et al., 2020; Ming

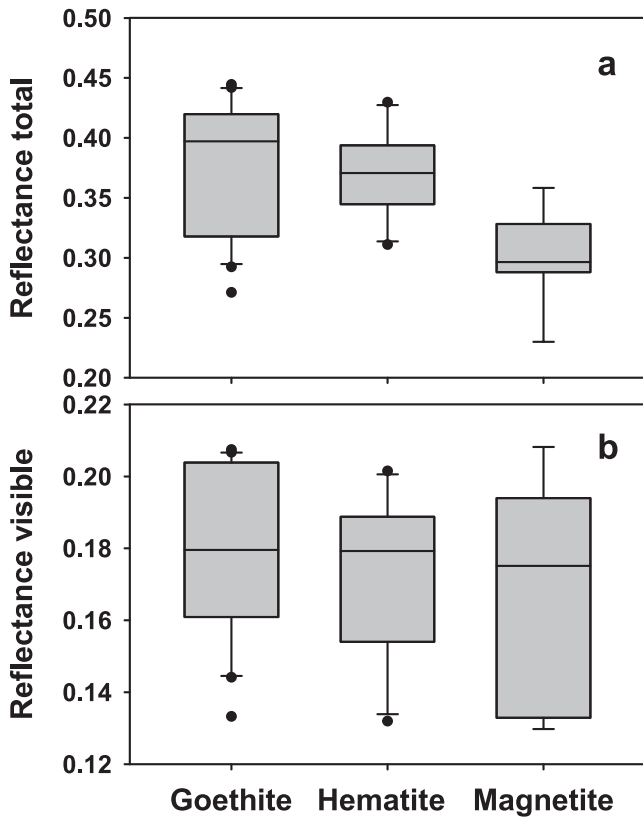


Figure 11. Box plots showing average total (a) and visible (b) reflectance values plotted by dominant iron oxide mineral.

& Wang, 2021; Revell et al., 2021). The different types of organic matter occurred in each sample but in varying unquantified amounts; therefore, the direct radiative forcing influences of the many forms of carbonaceous matter, including BC, were not assessed. Recently, Gleason et al. (2022) showed the importance of BC in promoting diminished albedo in mountain snow cover of the American West, including the UCRB, from 2015 to 2018. A detailed comparison of their results with ours is inadvisable because their BC determinations were made on size splits of 0.09–0.6 μm after excluding dust particles $>20 \mu\text{m}$ from snow-column-integrated samples under approximately maximal snow-water equivalent conditions and not ALM layers.

4.3.2. Dark Rock Particles and Other Hosts for Magnetite

Dark rock and mineral particles are implicated as an influence on diminished R_{tot} by the correspondence between R_{tot} and IRM. Because magnetite abundance was very low ($<0.38 \text{ wt. } \%$), it cannot by itself account for R_{tot} suppression. Instead, magnetite abundance is considered a proxy for dark rock and mineral particles, which were ubiquitous but variably abundant. Magnetite occurred within rock fragments having much greater surface area than the magnetite in them (Figure S8 in Supporting Information S1), as individual rock-derived magnetite grains commonly associated with ilmenite and other titaniferous minerals and as particles from pollutant emissions, such as fly ash. Anthropogenic, aggregated magnetite nanoparticles, not sought in this study, may also have contributed to diminished R_{tot} (see Moteki et al., 2017).

4.3.3. Ferric Oxide Minerals

Ferric oxide minerals of different sizes, origins, and occurrences were observed in each sample, likely suppressing R_{vis} but systematically so over time at only two sites—SASP and Wolf Creek Pass. These two southwestern-most sites are the closest ones to ferric oxide-bearing (both hematite and goethite) dust-source sediments of the southern Colorado Plateau. Detailed spectral reflectance, magnetic property, Mössbauer data as well as stereomicroscopic and SEM observations on six SASP samples (water years 2011–2016) were discussed by Reynolds et al. (2020) and contribute to the following general statements. The most common occurrences of microcrystalline and nano-size ferric oxide occurred in and on clay coats on quartz grains. Where examined, all iron-bearing clay coats contained discrete nano-size ferric oxide minerals as found in other dusts and dust-source sediments (Moskowitz et al., 2016; Reynolds, Cattle, et al., 2014). Very fine-grained ferric oxide minerals occurred within

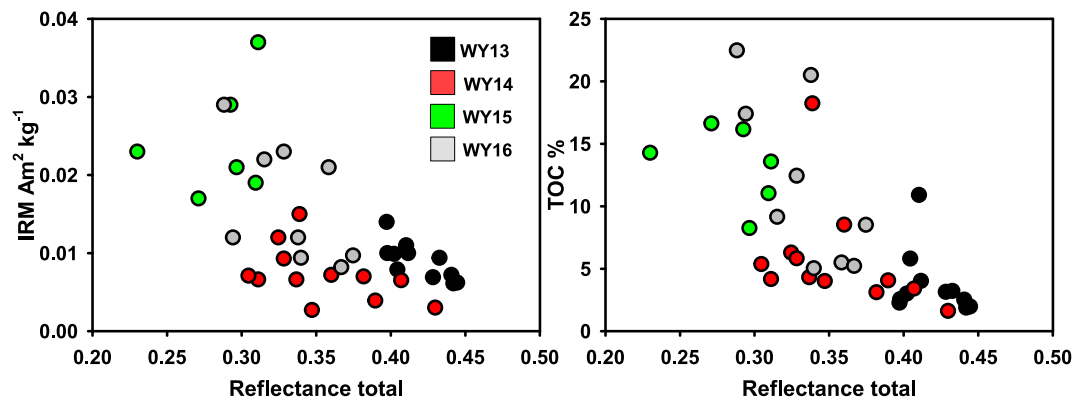


Figure 12. Plots of average total reflectance against (a) isothermal remanent magnetization (IRM; $r^2 = 0.37$) and (b) total organic carbon (TOC wt. %; $r^2 = 0.47$) by water years 2013–2016.

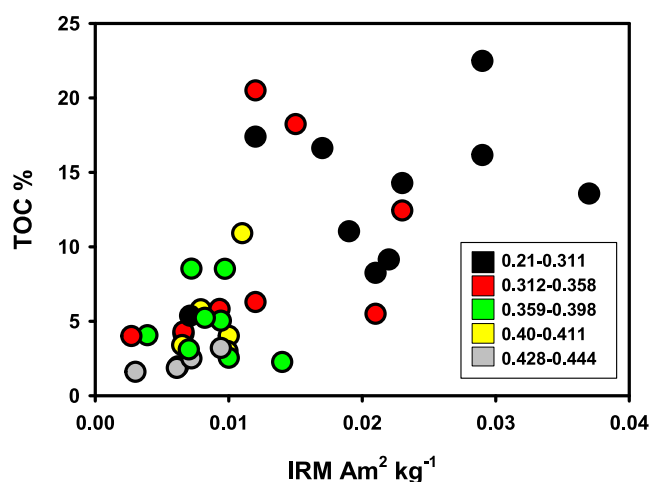


Figure 13. Plot of total organic carbon (TOC wt. %) versus isothermal remanent magnetization (IRM). Marker colors denote ranges in average total reflectance (Rtot) that were defined based on mostly separated clusters of Rtot values.

compositional attenuation of individual dust layers, the compositions of ALM samples retained a signature, revealed by the presence of a dominant iron oxide mineral, indicating annual dominance of some source regions over others at each site.

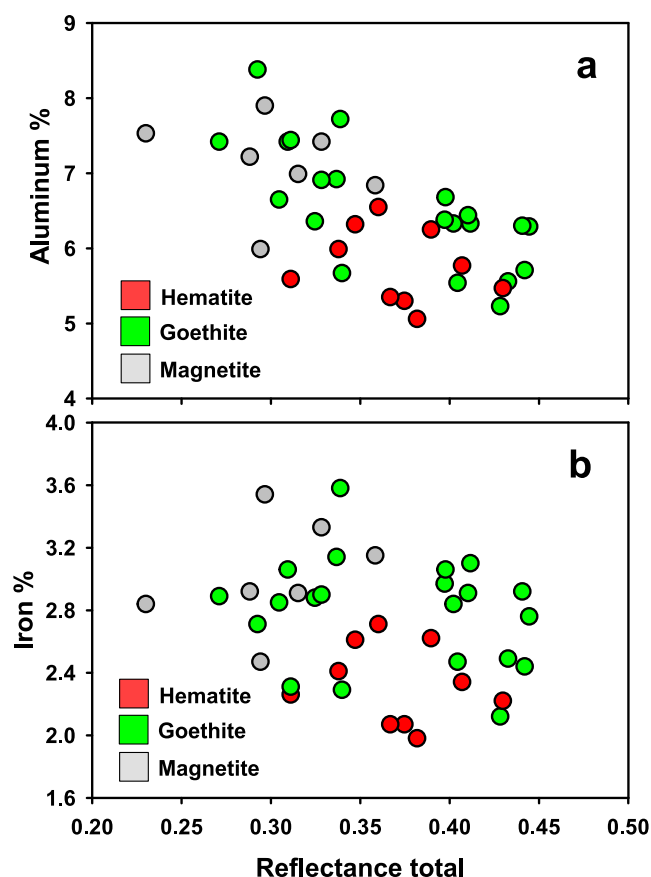


Figure 14. Plots of total reflectance against (a) aluminum wt. % ($r^2 = 0.40$) and (b) iron wt. % ($r^2 = 0.07$).

and on the surfaces of oxidized typically orange-to red-colored rock particles. Relatively coarse-grained, specular hematite was present with magnetite within rock fragments.

4.4. Causes of Variations in Spectral Reflectance

The interannual variations in Rtot values in ALM samples (Figure 2) are attributed to variable amounts of different LAPs from different source regions and types. Most ALM matter is ascribed to mineral dust from western North American desert surfaces delivered by discrete windstorms to snow surfaces resulting in individual dust layers during the period of snow accumulation (<http://www.codos.org/#codos>; accessed 25 April 2024). The compositions of these layers varied greatly in a study of 25 such layers (WY2011-16) at SASP (Reynolds et al., 2020). Nevertheless, the corresponding ALM layers there possessed much less compositional variability among water years than did the individual ALM layers produced by dust storms. The similar compositions of those ALM samples, the most important dust layer affecting snow melt, apparently represented an integration of variable compositions of individual dust layers deposited during a given water year. Reasonably, the properties of the ALM layers described here underwent similar compositional smoothing of individual dust layers deposited annually at a site. Despite such suspected

Importantly, the lack of consistency among ALM Rtot and Rvis values is ascribed to interannual variability in the sources for atmospheric PM (Figure 3). In this respect, a control on ALM properties was the proportion of dust from desert sources compared with background and fugitive sources. Most dust from lithogenic sediment at desert sources consists of silicate minerals. Such mineral dust can dilute the strong radiative forcing effects of certain anthropogenic LAPs, such as BC generated by industrial and transportation sectors (Reynolds et al., 2020). Evidence for these effects is found in the unusual properties of the WY15 suite having the lowest Rtot as well as highest amounts of magnetite, TOC, and most metals relative to those of the WY13 and 14, especially, and many parameters measured for the WY16 suite. The dilution of LAPs was demonstrated in the SASP WY11-16 ALM record in which Rtot and Rvis correlated with ALM mass loading (Reynolds et al., 2020). In that record, highest reflectance values were measured in high-mass ALM (50 g m^{-2} mainly from two massive WY13 dust storms in April (<http://www.codos.org/#codos>; accessed 25 April 2024). The lowest reflectance values were measured in the WY15 ALM having relatively low amounts of wind-storm dust (5.6 g m^{-2}) and highest amounts of mass-normalized LAPs. Across the region in the current study, WY15 was similarly characterized by few discrete dust layers. The ALM-sample properties of the current WY15 suite are similarly explained: WY15 ALM samples contained high amounts of LAP-bearing background fallout relative to ALM samples for the other years that contained proportionately more dust from regional dust storms.

The foregoing interpretation is strengthened by data showing that, for some samples, their late Julian days of collection were associated with high amounts of metals. That is, the final ALM layers at the time of collection contained, besides mostly desert dust, added PM in amounts roughly commensurate with the duration of ALM exposure at the surface. These observations appear to be consistent with data from daily sampling and

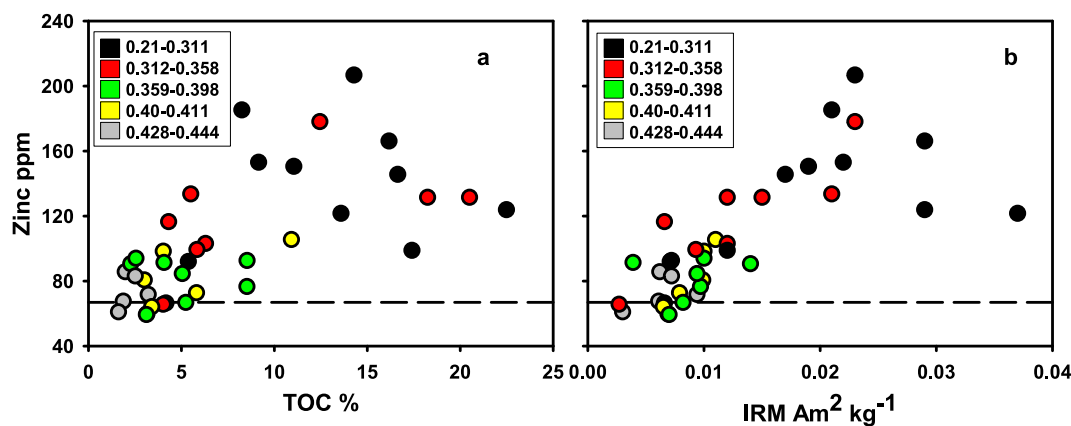


Figure 15. Bivariate plots of (a) zinc versus total organic carbon (TOC wt. %, $r^2 = 0.41$) and (b) zinc versus isothermal remanent magnetization (IRM, $r^2 = 0.57$). Marker colors denote ranges of average total reflectance (R_{tot}), from black, indicating a range of lowest R_{tot} , to gray, a range of highest R_{tot} . Dashed line, average UCC value for zinc (67 ppm).

measurement of snow layers collected at SASP revealing increases in BC in surface snow and dust concentrations after Julian day 120 during WY13 (Skiles & Painter, 2017). Two general sources might be responsible for the added LAPs: (a) fugitive particulates and (or) undetected late-season wind-event dust fall directly onto the ALM layer and (b) fugitive particulates scavenged from below by the ALM layer as it descended by melting into remaining snowpack. Elevated metals in late-collected snow may be largely attributable to anthropogenic emissions.

4.5. Compositions of Light Absorbing Particles Bearing on Dust Sources

Recent studies of dust generated within the interior American West have recognized many dryland dust-source regions on the basis of ground observations, satellite retrievals, back trajectory and meteorological analyses as well as some dust compositional attributes (Aarons et al., 2017; Axson et al., 2016; Carling et al., 2012, 2020; Dhital et al., 2024; Goodman et al., 2019; Hahnenberger & Nicoll, 2012, 2014; Hand et al., 2012, 2016, 2017; Heindel et al., 2020; Kandakji et al., 2020; Mangum et al., 2024; Miller et al., 2012; Munroe et al., 2019, 2023; Neff et al., 2013; Phillips & Doesken, 2011; Reynolds, Goldstein, et al., 2014, 2016, 2020; Skiles et al., 2015). Results herein provide additional compositional information to guide future recognition of desert source-area locations and behavior, including their interannual changes across the American West. More detailed knowledge about source areas, types, conditions, and behaviors can be achieved when ALM compositions are compared with candidate source-sediment compositions and then reasonably well-matched data are evaluated under regional assessments of land cover-land use (e.g., Duniway et al., 2019; Li et al., 2013; Mangum et al., 2024; Munson et al., 2011; Nauman et al., 2018, 2023; Tyree et al., 2024), all supported by satellite retrievals and back trajectory analysis (e.g., Axson et al., 2016; Munroe et al., 2023; Skiles et al., 2015). Compositional evidence also

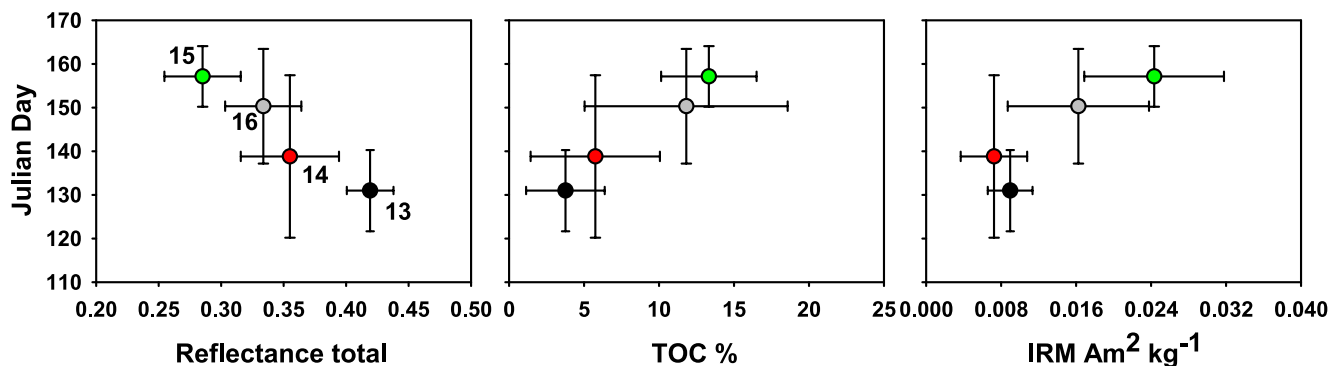


Figure 16. Julian days of sample collection by water years versus average total reflectance, total organic carbon (TOC wt. %), and isothermal remanent magnetization (IRM) plotted as their means with standard deviations represented by error bars.

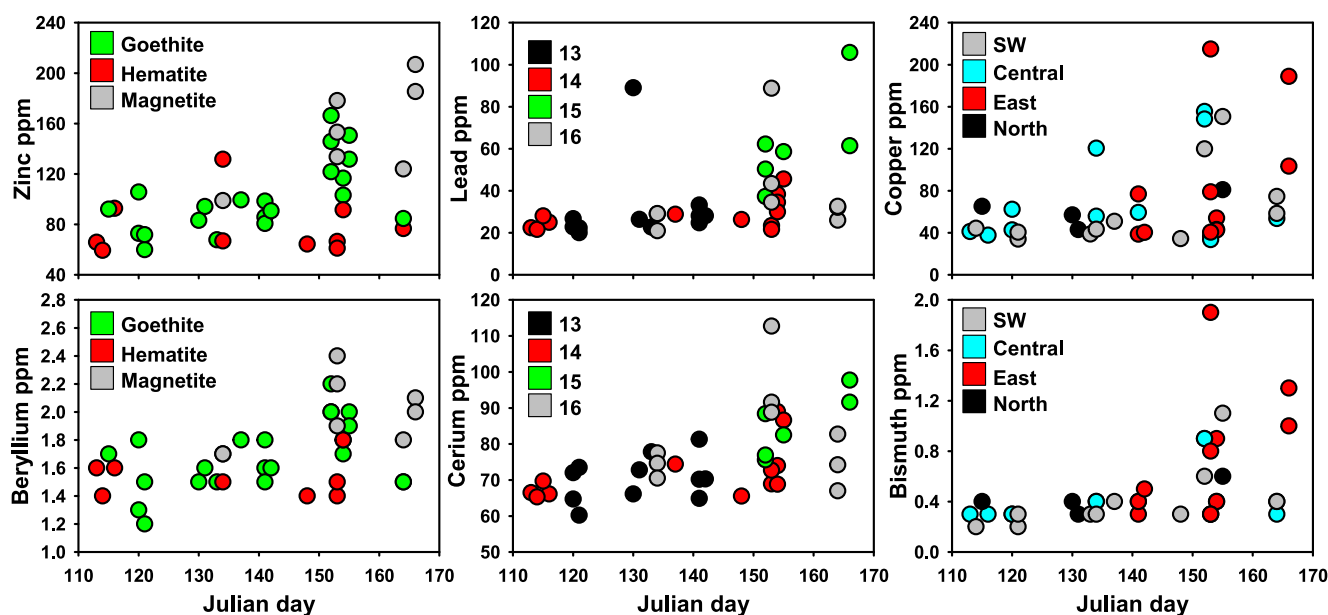


Figure 17. Julian days of collection versus trace elements by iron oxide group, water year, and location as noted in legends.

points to many diffuse sources of anthropogenic dusts (see Reynolds et al., 2010, 2014a, 2020, 2024; Carling et al., 2012; Dastrup et al., 2018; Goodman et al., 2019; Heindel et al., 2020; Munroe et al., 2019).

The three iron oxide-mineral groups retained distinct mineralogic and chemical signatures, which signified fundamental differences in source-sediment mineralogy (Table 3, eg., Figure S9 in Supporting Information S1). In addition, the particle-size differences among the three iron oxide groups likely arose partly from different dust-transport distances, but they also apparently varied as functions of the textures of sedimentary bedrock, the weathering of which produced most dust-source sediments. For example, preliminary data indicate that dust-source sediments derived from marine mudstones in northwestern New Mexico contain goethite as the only ferric oxide identified by reflectance spectroscopy. We thus surmise that the overall fine-grained characteristics of the goethite-group samples derived at least partly from goethite-bearing, clay-rich Cretaceous sedimentary rocks primarily south and southwest of the UCRB study region. Using spectral reflectance methods, determination of the dominant iron oxide in surficial sediments at known or suspected dust sources might generate a mapped guide to help discriminate among primary sources for individual dust layers and ALM layers.

The associations among certain metals and REE, IRM, and TOC indicate multiple origins for LAPs: sediments derived from different bedrock types; emissions from fossil-fuel combustion for stationary power generation, emissions related to transportation involving tailpipe particulates, debris from tire, road, and vehicle wear, mining activities (processing, smelting, reclamation, roads, and wastes), waste-water treatment as well as deteriorated metalliferous infrastructure and waste. Few of the measured trace elements, separately or combined, are unique to their sources, making difficult precise attributions with the current data.

Roads and vehicles can be considered as related sources because together they can produce many recognized forms of LAPs and their associated trace elements. Road-tire wear produces micro and nanoplastic fragments (Bank & Hansson, 2019; Evangelidou et al., 2020; Hao et al., 2001; Kole et al., 2017; Sommer et al., 2018; Vogelsang et al., 2020; Wagner et al., 2018). These fragments consist of monomers and polymers homogeneously permeated by nano-size carbon black that imparts the black color to tires, thereby potentially promoting snowmelt (Reynolds et al., 2024). Far-distant, perhaps transoceanic, transport cannot be discounted for some microplastics in UCRB snow (e.g., Bergmann et al., 2019; Evangelidou et al., 2020; Zhang et al., 2019) nor can remote sources of microplastics from oceanic sea spray and bubble-burst actions (Allen et al., 2020; Trainic et al., 2020). Particulate emissions from motor vehicles associated with tailpipe emissions as well as brake and tire wear contain As, Ba, Cd, Ce, Cu, Sb, Sr, Pb, Zn, Al, Ca, Fe, Mg, and K in addition to forms of organic and elemental carbon (e.g., Adachi & Tainosho, 2004; Arca Bati & Altun, 2020; Chen et al., 2023; Dietl et al., 1997; Goddard et al., 2019; Grigoratos & Martini, 2015; Lough et al., 2005; Schauer et al., 2006). Barium, Ce, Nd, and La are fuel additives

Table 3
List of All-Layers-Merged (ALM) Sample Properties and Parameters According to the Influence by Dominant Iron Oxide Group

Parameter	Goethite	Hematite	Magnetite (n.d.)
Rtot	=	=	Lowest
Rvis	=	=	=
IRM	Mid	Lowest	Highest
HIRM	=	=	Lowest
ARM/IRM	=	=	Lowest
TOC	=	=	Highest
Al	Mid	Lowest	Highest
Fe	Mid	Lowest	Highest
K	=	=	Highest
Na	=	=	Highest
P	=	=	Highest
Mg	=	=	=
Ca	=	=	=
Cu	Mid	Lowest	Highest
Zn	Mid	Lowest	Highest
Pb	Mid	Lowest	Highest
Mo	Mid	Lowest	Highest
As	=	=	Highest
Ba	Mid	Lowest	Highest
Bi	Mid	Lowest	Highest
Ce	Mid	Lowest	Highest
La	Mid	Lowest	Highest
Cd	Mid	Lowest	Highest
Co	Mid	Lowest	Highest
Cr	Mid	Lowest	Highest
Cs	=	Lowest	=
Nb	Mid	Lowest	Highest
Ni	Mid	Lowest	Highest
Sc	Mid	Lowest	Highest
Sb	Mid	Lowest	Highest
Sr	Mid	Lowest	Highest
Rb	Mid	Lowest	Highest
U	Mid	Lowest	Highest
Th	Mid	Lowest	Highest
Tl	Mid	Lowest	Highest
Mn	=	=	Highest
Li	=	=	Highest
Nd	=	=	Highest
Ga	Mid	Lowest	Highest
K/Rb	Mid	Highest	Lowest
Median	Finest	Coarsest	Mid
PM2.5	Finest	=	=

that may be incorporated into soot (e.g., Turley et al., 1973). The many sources for magnetite include road wear of asphalt containing crushed magnetite-bearing rock and brake wear (Gonet et al., 2021; Gonet & Maher, 2019; Moteki et al., 2017).

Particulate matter from stationary, power generating coal, and oil combustion can be enriched in As, Ba, Be, Bi, Cd, Co, Cr, Cu, La, Mo, Mn, Ni, Pb, Rb, Sb, Sc, Sr, Tl, Th, and Zn as well as major elements Ca and Fe, along with several forms of organic matter, such as coal char and soot (Bragg et al., 1998; EPA, 1996; Finkelman et al., 2002; Olmez & Gordon, 1985; Senior et al., 2020). Zinc and Pb can be enriched in coal tars, a byproduct of coal combustion used as pavement sealants among other applications that degrade into fine PM (Van Metre et al., 2009).

Elements that may be linked to mining activities in the study area include Mo, Cu, Pb, and Zn. Although the large interannual variations in LAP amounts and most other constituents were not strongly expressed as geographic differences, a notable exception was the 4-year average of elevated Mo in East-sector samples. Within the East sector, deposits of Mo ore have been extracted from three mines, one inactive open-pit, and two active underground operations, with associated mine tailings, dirt roads, and ongoing reclamation. The Mo ores occur in magnetite-bearing rocks and are associated with Zn, Ce, La, U, Th, Nb, Sc, and Y (Audétat, 2015; Desborough & Mihalik, 1980) for which the averages of each were elevated in East-sector sites.

The significantly higher sand contents in samples from the east sites, compared with those in the other sectors, might be ascribed to a component of local dust in the east sector and linked to some metals from mining activities. The relation of high sand content with low ARM/IRM, overall and especially in most east-site samples, suggested the presence of relatively large magnetite particles in relatively coarse dust and was thus consistent with a local dust component (Figure S10 in Supporting Information S1). Elevated average Ce and Zn amounts in the east-site samples cloud the speculation about transportation-sector sources for these elements in these samples. Otherwise, average Ce and Zn amounts considered by the three other location-groups are closely similar.

With respect to particle size, dust from Asia might be considered a source for some amount of PM_{2.5} in the UCRB, inasmuch as Asian dust has been traced to North America, especially to its west coast (Creamean et al., 2014; Fairlie et al., 2007; Fischer et al., 2009; Husar et al., 2001; Kavouras et al., 2009; VanCuren & Cahill, 2002; Zhao et al., 2008). Asian dust, however, is likely a negligible component in the UCRB based on direct measurements and modeling that links regional dust-storm emissions and dynamics with deposition of PM_{2.5} and PM₁₀ (Achakulwisut et al., 2018; Hand et al., 2016, 2017; Munroe et al., 2023; Neff et al., 2013; Reynolds et al., 2016, 2020; Skiles et al., 2015).

4.6. Influence of Winter-Spring Dust on Mountain Ecosystems

Atmospheric dust can deliver essential nutrients to mountain soils and water bodies when ALM layers contact the surface (see Brahney et al., 2014; Carling et al., 2012; Checketts et al., 2020; Dastrup et al., 2018; Goodman et al., 2019; Heindel et al., 2020; Lawrence et al., 2010, 2013; Munroe et al., 2014; Zhang, Goldstein, et al., 2018). Considering P, its abundance was much higher in the magnetite-group samples primarily in the WY15 and 16

Table 3
Continued

Parameter	Goethite	Hematite	Magnetite (n.d.)
PM10	Finest	Coarsest	Mid
PM20-10	Finest	Coarsest	Mid
PM63	Finest	Mid	Coarsest
Sand	Finest	Mid	Coarsest

Note. The influences of the dominant iron oxide group ranked for highest, lowest, and in-between (Mid) values or amounts, or finest, coarsest, and in between (Mid) for particle sizes. Equal markers denote approximately equivalent effects, amounts, or texture. As examples, the magnetite-group samples generated overall lowest R_{tot} values, while possessing highest IRM and TOC but lowest HIRM and K/Rb values, the latter of which exemplified a mineralogic indicator for mica (Figure S9 in Supporting Information S1).

samples, but it varied greatly within each geographic sector. Potassium contents were similar to those of P in iron oxide and water-year groups.

The sources and fates of Ca-bearing minerals in ALM samples represent a special case for their potential value as a dust proxy and roles in buffering acid deposition. Amounts of Ca in these samples were far less than amounts in individual dust-on-snow layers at SASP (WY11-16) and the UCC average for Ca (Figure S11 in Supporting Information S1). Moreover, Ca amounts tended to decrease commensurately with later Julian days of collection (Figure S12 in Supporting Information S1). These results, and those of Clow and Ingersoll (1994), Clow et al. (2016), and Reynolds et al. (2020) indicating that Ca was depleted during its residence in snow cover, preclude the application of Ca abundance as a derivative dust proxy in lake sediments when compared with Ca in snow samples taken during the melt season (spring and early summer) in the North American Mountain West (cf., Arcusa et al., 2019; Routson et al., 2019). As with many other properties, P-Ca relations differed in the WY13-14 samples compared with the WY15-16 samples, the latter group following a general trend of increased P with greater Ca (Figure S11 in Supporting Information S1).

5. Implications, Uncertainties, and Questions

Results from this study, indicating that WY2013-16 ALM average total reflectance values varied overall by a factor of nearly two, imply a roughly similar range for contemporaneous interannual variations in late season snow-surface albedo (SSA) across the UCRB (Figure 3; Table S9 in Supporting Information S1). This variation reflects differences in amounts and types of LAPs but no other important factors such as snow metamorphic effects. Meaningful comparison among previous measurements of direct LAP radiative forcing, LAP optical properties, derived SSA (Skiles et al., 2012, 2015, 2017, 2018; Jensen et al., 2024; Painter, Skiles, et al., 2012; Skiles & Painter, 2017), and our reflectance measurements await in-depth analyses. Nevertheless, the results imply that LAP-induced SSA of one or several ALM layers from 1 year would not capture the albedo effects of atmospheric PM across the UCRB over several years, thereby underscoring the value of continued study of UCRB-ALM compositions and of radiative forcing monitoring across the UCRB (see Jensen et al., 2024).

Uncertainties associated with each of the LAP classes—carbonaceous matter, dark rock and mineral particles, and ferric oxide minerals—leave much to be learned about the effects of BC and mineral dust on UCRB snow melt. The efficacy of snow-radiation modeling would be enhanced by the following: (a) identification of the numerous types of carbonaceous matter and quantification of their amounts, (b) systematic investigation of the radiative forcing influences of dark rock particles from their natural and anthropogenic sources, and (c) improved measures of the optical properties of the ferric oxide minerals (cf., Di Biagio et al., 2019, 2020; Go et al., 2021; Zhang et al., 2015) to include their common nano-size occurrences. With respect to snow radiative modeling, in addition, we note that particle sizes (e.g., median sizes) in regional dust deposited to UCRB snow are much coarser than those considered in prior modeling studies (e.g., Oaida et al., 2015; Skiles et al., 2017) that used a maximum particle size of 6 μm .

The results raise questions about the causes of variations in the amounts and compositions of LAPs in the ALM samples. To what extent do the observed interannual variations in LAPs represent variability in dominant source-area contributions caused by changes in source-area conditions, and to what extent do they indicate changes in dust-storm patterns and strengths? Do the compositional similarities of WY15 and 16 compared with WY13 and 14 samples represent a fundamental shift in regional source locations and behavior? This question may be addressed by back trajectory analyses (not done here; see 2010–2013 examples in Skiles et al., 2015). Are some microplastics delivered to the UCRB by transoceanic transport, considering the observations of microplastics on arctic ice flows and in other polar settings (Aves et al., 2022; Bergmann et al., 2019)? What, in detail, are the anthropogenic sources of many trace elements as indicated by their elevated amounts relative to their UCC averages? Bundling some of these questions, what are the specific contributions of road-tire-wear particles to radiative forcing of snow cover? With respect to dust in mountain ecosystems, what are the types, pedogenic fates, and environmental effects of phosphorus, iron, calcium, and tire matter under different soil and hydrologic settings (see Brahney et al., 2013, 2014; Scholz & Brahney, 2022; Zhang, Z. et al., 2018)? Do some LAPs undergo

mineralogic and chemical changes during atmospheric transport even over the relatively short regional distances of a few hundred km? Regarding the prediction of river flows, how important are the relative proportions of different LAPs compared to the amount of dust and its exposure time, a question that could be addressed in conjunction with the Colorado Basin River Forecast Center (<https://www.cbrfc.noaa.gov/lmap/lmap.php>; accessed 15 October 2024)? These questions offer gateways to further research.

6. Conclusions

The LAP classes that diminished laboratory-measured spectral reflectance as an indicator of radiative forcing were different types of carbonaceous matter, dark rock and mineral particles as well as ferric oxide minerals. Each class of LAP was found in each sample. Differences in LAP amounts and thus their relative radiative effects led to differences in reflectance by water years, but quantitative attribution of a particular LAP component to diminished reflectance was uncertain for any sample, group of samples or for the entire sample suite. The radiative forcing effects of dark rock and mineral particles have been previously overlooked for their roles in structuring snow- and ice-surface albedo. With respect to global dust models, consideration of the radiative forcing effects of dark rock and mineral particles might improve estimates of atmospheric responses to global dust loading. The many kinds and sources of carbon included forms of black carbon, some types of which were inferred as soot from fossil-fuel combustion by the association of carbon with trace-metal abundances exceeding their average amounts in the upper continental crust. Particles generated by road-tire wear constitutes another black carbonaceous component that likely diminished spectral reflectance. More detailed characterization of all carbonaceous matter would lead to better understanding of its radiative forcing effects. Ferric oxide minerals were also implicated for their radiative forcing effects but to subordinate effect relative to those of carbonaceous and black rock and mineral particles.

The results may help guide studies to identify desert sources for LAPs in UCRB snow. Dominant iron oxide mineral, whether goethite or hematite as identified by spectral reflectance or magnetite determined by magnetic properties, was a primary discriminator for ALM compositional and textural differences. Such differences are interpreted to indicate proportionally different source-area contributions, which varied primarily by water year. The causes for such interannual differences are amenable to deeper examination with respect to dust-storm frequency and tracks. Future results on LAPs in post-WY2016 snow samples, combined with the WY2013-16 data, would enable evaluation of compositional influences by climatic factors, such as ENSO and PDO, to the extent that such factors partly control dust activity (Hand et al., 2017).

Identification of dust-source areas is a practical matter. At this point, different UCRB ALM-snow compositions are insufficiently diagnostic of specific desert-source locations as point sources on the order of a few km². When such diagnoses are achieved, recurrently active sources may be considered for mitigation to confer downwind benefits to water-resource management and human health. Dust from widespread anthropogenic sources complicates the goals of geographic source attribution, so that the issues of such fugitive dust confound prospects for short-term mitigation.

In addition to the potential value of linking properties of ALM samples to water-resource management, future examination of these properties would provide valuable information about several other issues. The ecological effects from early snowmelt (Steltzer et al., 2009) and ensuing pulses of potential nutrients, acid buffers, minerals, metals, microplastics, and tire matter to soil, streams, and lakes when the ALM layer contacts the ground surface await detailed study in sensitive areas. In particular, the toxic effects of tire matter on mountain organisms are largely unknown (see Greer et al., 2023; Tian et al., 2021). Dust properties may also be evaluated as nuclei for cloud condensation and ice formation (Zimmermann et al., 2008). Moreover, interannual changes in the properties of ALM samples may reveal ongoing changes in landscape conditions in dry and drying western North America. Finally, the particle-size distributions of ALM samples may capture the levels and trends of regional air pollution during winter and most of springtime. These assessments might aid estimation and prediction of potential health effects of dust among communities in and astride the Colorado Rocky Mountains (e.g., Achakulwisut et al., 2018, 2019; Crooks et al., 2016; Ghio et al., 2014; Neff et al., 2013; Reynolds et al., 2016; Zhang et al., 2016).

A general explanation for variable compositions of the ALM samples is that strong, regional winds swept up loose, fine-grained matter from diverse landscapes over large areas of western United States. The land-surface sources were both natural and disturbed. Direct emissions of atmospheric PM from anthropogenic activities

were also involved. With snowpack melting, the ALM layers mixed all individual wind-blown dust and non-windstorm-related background PM, thereby integrating compositions from multiple sources during winter-early spring. Most ALM mass comes from deserts, providing many LAPs, based on direct observations, satellite retrievals, mineralogy, chemical and physical composition, and modeling. Nevertheless, a measurable proportion of radiative forcing driving snow melt is attributed to many anthropogenic sources.

Conflict of Interest

The authors declare no conflicts of interest relevant to this study.

Data Availability Statement

Data, observations, and metadata supporting the conclusions can be obtained in Supporting Information and in the ScienceBase database, <https://doi.org/10.5066/P13HIOO8> (Goldstein et al., 2024; published 22 July 2024). Metadata include identification information, data quality information, spatial reference information, entity and attribute information, distribution information, and metadata reference information. For location information, the Geodetic Model used the Horizontal Datum WGS84 and Ellipsoid GRS_1980.

Acknowledgments

We are grateful to Jiang Xiao, Eric Fisher, and Michael Sirls for laboratory analyses, Chris Landry and Andrew Temple for sample collection 2011–2015, and Paco Van Sistene for preparation of Figure 1. Reviews by Greg Carling, Saroj Dhital, and three anonymous reviewers are deeply appreciated. Any use of trade, firm, or product names is for descriptive purposes only and does not imply endorsement by the U.S. Government. The Institute for Rock Magnetism (IRM) is a U.S. National Multiuser Facility supported through the Instrumentation and Facilities program of the National Science Foundation, Earth Sciences Division, award NSF-EAR 2153786, and by funding from the University of Minnesota. This is IRM publication number 2402. This study was supported by the Ecosystems Land Change Science Program of the U.S. Geological Survey.

References

- Aarons, S. M., Blakowski, M. A., Aciego, S. M., Stevenson, E. I., Sims, K. W. W., Scott, S. R., & Aarons, C. (2017). Geochemical characterization of critical dust source regions in the American West. *Geochimica et Cosmochimica Acta*, 215, 141–161. <https://doi.org/10.1016/j.gca.2017.07.024>
- Achakulwisut, P., Anenberg, S. C., Neumann, J. E., Penn, S. L., Weiss, N., Crimmins, A., et al. (2019). Effects of increasing aridity on ambient dust and public health in the U.S. southwest under climate change. *GeoHealth*, 3(5), 127–144. <https://doi.org/10.1029/2019GH000187>
- Achakulwisut, P., Mickley, L. J., & Anenberg, S. C. (2018). Drought-sensitivity of fine dust in the US Southwest: Implications for air quality and public health under future climate change. *Environmental Research Letters*, 13(5), 054025. <https://doi.org/10.1088/1748-9326/aabf20>
- Adachi, K., & Tainosho, Y. (2004). Characterization of heavy metal particles embedded in tire dust. *Environment International*, 30(8), 1009–10117. <https://doi.org/10.1016/j.envint.2004.04.004>
- Alfaro, S. C., Lafon, S., Rajot, J. L., Formenti, P., Gaudichet, A., & Maille, M. (2004). Iron oxides and light absorption by pure desert dust: An experimental study. *Journal of Geophysical Research*, 109(D8), D08208. <https://doi.org/10.1029/2003JD004374>
- Allen, S., Allen, D., Karbalaee, S., Maselli, V., & Walker, T. R. (2022). Micro (nano) plastics sources, fate, and effects: What we know after ten years of research. *Journal of Hazardous Materials Advances*, 6, 100057. <https://doi.org/10.1016/j.hazadv.2022.100057>
- Allen, S., Allen, D., Moss, K., Le Roux, G., Phoenix, V. R., & Sonke, J. E. (2020). Examination of the ocean as a source for atmospheric microplastics. *PLoS One*, 15(5), e0232746. <https://doi.org/10.1371/journal.pone.0232746>
- Allen, S., Allen, D., Phoenix, V. R., Le Roux, G., Durántez Jiménez, P., Simonneau, A., et al. (2019). Atmospheric transport and deposition of microplastics in a remote mountain catchment. *Nature Geoscience*, 12(5), 339–344. <https://doi.org/10.1038/s41561-019-0335-5>
- Arca Bati, Z., & Altun, S. (2020). Investigation of the effect of barium-based additive on smoke and NOx emissions of a diesel engine fueled with conventional and biodiesel fuels. *Clean Technologies and Environmental Policy*, 22(6), 1285–1295. <https://doi.org/10.1007/s10098-020-01869-0>
- Arcusa, S. H., McKay, N. P., Routson, C. C., & Munoz, S. E. (2019). Dust-drought interactions over the last 15,000 years: A network of lake sediment records from the san juan mountains, Colorado. *The Holocene*, 30(4), 559–574. <https://doi.org/10.1177/0959683619875192>
- Audétat, A. (2015). Climax mine compositional evolution and formation conditions of magmas and fluids related to porphyry Mo Mineralization at Climax, Colorado. *Journal of Petrology*, 56(8), 1519–1546. <https://doi.org/10.1093/petrology/egv044>
- Aves, A. R., Revell, L. E., Gaw, S., Ruffell, H., Schuddeboom, A., Wotherspoon, N. E., et al. (2022). First evidence of microplastics in Antarctic snow. *The Cryosphere*, 16(6), 2127–2145. <https://doi.org/10.5194/tc-16-2127-2022>
- Axson, J. L., Shen, H., Bondy, A. L., Landry, C. C., Welz, J., Creamean, J. M., & Ault, A. P. (2016). Transported mineral dust deposition case study at a hydrologically sensitive mountain site: Size and composition shifts in ambient aerosol and snowpack. *Aerosol and Air Quality Research*, 16(3), 555–567. <https://doi.org/10.4209/aaqr.2015.05.0346>
- Bank, M. S., & Hansson, S. V. (2019). The plastic cycle: A novel and holistic paradigm for the anthropocene. *Environmental Science and Technology*, 53(13), 7177–7179. <https://doi.org/10.1021/acs.est.9b02942>
- Bergmann, M., Mützel, S., Primpke, S., Tekman, M. B., Trachsel, J., & Gerdt, G. (2019). White and wonderful? Microplastics prevail in snow from the Alps to the arctic. *Science Advances*, 5(8). <https://doi.org/10.1126/sciadv.aax1157>
- Bond, T. C., & Bergstrom, R. W. (2006). Light absorption by carbonaceous particles: An investigative review. *Aerosol Science and Technology*, 40(1), 27–67. <https://doi.org/10.1080/02786820500421521>
- Bond, T. C., Doherty, S. J., Fahey, D. W., Forster, P. M., Berntsen, T., DeAngelo, J., et al. (2013). Bounding the role of black carbon in the climate system: A scientific assessment. *Journal of Geophysical Research: Atmospheres*, 118(11), 5380–5552. <https://doi.org/10.1002/jgrd.50171>
- Bragg, L. J., Oman, J. K., Tewalt, S. J., Oman, C. L., Rega, N. H., Washington, P. M., & Finkelman, R. B. (1998). *U.S. Geological Survey coal quality (COALQUAL) database: Version 2.0* (pp. 97–134). U.S. Geological Survey Open-File Report.
- Brahney, J., Ballantyne, A. P., Kociolek, P., Spaulding, S., Otu, M., Porwoll, T., & Neff, J. C. (2014). Dust mediated transfer of phosphorus to alpine lake ecosystems of the Wind River Range, Wyoming, USA. *Biogeochemistry*, 120(1), 259–278. <https://doi.org/10.1007/s10533-014-9994-x>
- Brahney, J., Ballantyne, A. P., Sievers, C., & Neff, J. C. (2013). Increasing Ca²⁺ deposition in the western US: The role of mineral aerosols. *Aeolian Research*, 10, 77–87. <https://doi.org/10.1016/j.aeolia.2013.04.003>
- Brahney, J., Hallerud, M., Heim, E., Hahnberger, M., & Sukumar, S. (2020). Plastic rain in protected areas of the United States. *Science*, 368(6496), 1257–1260. <https://doi.org/10.1126/science.aaz5819>

- Brahney, J., Mahowald, N., Prank, M., Cornwell, G., Klimont, Z., Matsui, H., & Prather, K. A. (2021). Constraining the atmospheric limb of the plastic cycle. *Proceedings of the National Academy of Sciences*, *118*(16). <https://doi.org/10.1073/pnas.2020719118>
- Briggs, P. H. (2002). The determination of forty elements in geological and botanical samples by inductively coupled plasma-atomic emission spectrometry. In J. E. Taggart (Ed.), *Analytical methods for chemical analysis of geologic and other materials* (p. 11e114). U.S. Geological Survey Open-File Report 02e223.
- Briggs, P. H., & Meier, A. L. (2002). The determination of forty-two elements in geological materials by inductively coupled plasma-mass spectrometry. In J. E. Taggart (Ed.), *Analytical methods for chemical analysis of geologic and other materials*, pp. 11e114. U.S. Geological Survey open-file report 02-223.
- Carling, G. T., Fernandez, D. P., & Johnson, W. P. (2012). Dust-mediated loading of trace and major elements to Wasatch Mountain snowpack. *Science of the Total Environment*, *432*, 65–77. <https://doi.org/10.1016/j.scitotenv.2012.05.077>
- Carling, G. T., Fernandez, D. P., Rey, K. A., Hale, C. A., Goodman, M. M., & Nelson, S. T. (2020). Using strontium isotopes to trace dust from a drying Great Salt Lake to adjacent urban areas and mountain snowpack. *Environmental Research Letters*, *15*(11), 114035. <https://doi.org/10.1088/1748-9326/abbfc4>
- Carling, G. T., Tingey, D. G., Fernandez, D. P., Nelson, S. T., Aanderud, Z. T., Goodsell, T. H., & Chapman, T. R. (2015). Evaluating natural and anthropogenic trace element inputs along an alpine to urban gradient in the Provo River, Utah, USA. *Applied Geochemistry*, *10*, 398–412. <https://doi.org/10.1016/j.apgeochem.2015.10.005>
- Checketts, H. N., Carling, G. T., Fernandez, D. P., Nelson, S. T., Rey, K. A., Tingey, D. G., et al. (2020). Trace element export from the critical zone triggered by snowmelt runoff in a Montane Watershed, Provo river, Utah, USA. *Frontiers in Water*, *2*, 578677. <https://doi.org/10.3389/frwa.2020.578677>
- Chen, S., Chen, J., Zhang, Y., Lin, J., Bi, H., Song, H., et al. (2023). Anthropogenic dust: Sources, characteristics and emissions. *Environmental Research Letters*, *18*(10), 103002. <https://doi.org/10.1088/1748-9326/acf479>
- Clark, R. N. (1983). Spectral properties of mixtures of montmorillonite and dark carbon grains: Implications for remote sensing minerals containing chemically and physically adsorbed water. *Journal of Geophysical Research*, *88*(B12), 10635–10644. <https://doi.org/10.1029/jb088ib12p10635>
- Clements, N., Eav, J., Xie, M., Hannigan, M. P., Miller, S. L., Navidi, W., et al. (2014). Concentrations and source insights for trace elements in fine and coarse particulate matter. *Atmospheric Environment*, *89*, 373–381. <https://doi.org/10.1016/j.atmosenv.2014.01.011>
- Clow, D. W., & Ingersoll, G. I. (1994). Particulate carbonate matter in snow from selected sites in the south-central Rocky Mountains. *Atmospheric Environment*, *28*(4), 575–584. [https://doi.org/10.1016/1352-2310\(94\)90033-7](https://doi.org/10.1016/1352-2310(94)90033-7)
- Clow, D. W., Williams, M. W., & Schuster, P. W. (2016). Increasing aeolian dust deposition to snowpacks in the Rocky Mountains inferred from snowpack, wet deposition, and aerosol chemistry. *Atmospheric Environment*, *146*, 183–194. <https://doi.org/10.1016/j.atmosenv.2016.06.076>
- Cowger, W., Booth, A. M., Hamilton, B. M., Thaysen, C., Primpke, S., Munno, K., et al. (2020). Reporting guidelines to increase the reproducibility and comparability of research on microplastics. *Applied Spectroscopy*, *74*(9), 1066–1077. <https://doi.org/10.1177/0003702820930292>
- Creamean, J. M., Spackman, J. R., Davis, S. M., & White, A. B. (2014). Climatology of long-range transported Asian dust along the west coast of the United States. *Journal of Geophysical Research*, *119*(21), 12171–12185. <https://doi.org/10.1002/2014JD021694>
- Crooks, J. L., Cascio, W. E., Percy, M. S., Reyes, J., Neas, L. M., & Hilborn, E. D. (2016). The association between dust storms and daily non-accidental mortality in the United States, 1993–2005. *Environmental Health Perspectives*, *124*(11), 1735–1743. <https://doi.org/10.1289/EHP216>
- Dang, C., Warren, S. G., Fu, Q., Doherty, S. J., Sturm, M., & Su, J. (2017). Measurements of light-absorbing particles in snow across the Arctic, North America, and China: Effects on surface albedo. *Journal of Geophysical Research: Atmospheres*, *122*(19), 10149–10168. <https://doi.org/10.1002/2017JD027070>
- Dastrup, D. B., Carling, G. T., Collins, S. A., Nelson, S. T., Fernandez, D. P., Tingey, D. G., et al. (2018). Aeolian dust chemistry and bacterial communities in snow are unique to airshed locations across northern Utah, USA. *Atmospheric Environment*, *193*, 251–261. <https://doi.org/10.1016/j.atmosenv.2018.09.016>
- Deems, J., Painter, T. H., Barsugli, J., Belnap, J., & Udall, B. (2013). Combined impacts of current and future dust deposition and regional warming on Colorado River Basin snow dynamics and hydrology. *Hydrology and Earth System Sciences*, *17*(11), 4401–4413. <https://doi.org/10.5194/hess-17-4401-2013>
- Derimian, Y., Karnieli, A., Kaufman, Y. J., Andreae, M. O., Andreae, T. W., Dubovik, O., et al. (2008). The role of iron and black carbon in aerosol light absorption. *Atmospheric Chemistry and Physics*, *8*(13), 3623–3637. <https://doi.org/10.5194/acp-8-3623-2008>
- Desborough, G. A., & Mihalik, P. (1980). Accessory minerals in the igneous host of Molybdenum ore, Henderson mine, Colorado. *USGS Open-file Report*, 80–661, 19. <https://pubs.usgs.gov/of/1980/0661/report.pdf>
- Dhital, S., Webb, N. P., Chappell, A., Kaplan, M. L., Nauman, T. W., Tyree, G., et al. (2024). Synoptic analysis and WRF-Chem model simulation of dust events in the southwestern United States. *Journal of Geophysical Research: Atmospheres*, *129*(13), e2023JD040650. <https://doi.org/10.1029/2023jd040650>
- Di Biagio, C., Balkanski, Y., Albani, S., Boucher, O., & Formenti, P. (2020). Direct Radiative Effect by mineral dust aerosols constrained by new microphysical and spectral optical data. *Geophysical Research Letters*, *47*(2), 1–12. <https://doi.org/10.1029/2019GL086186>
- Di Biagio, C., Formenti, P., Balkanski, Y., Caponi, L., Cazaunau, M., Pangui, E., et al. (2019). Complex refractive indices and single scattering albedo of global dust aerosols in the shortwave spectrum and relationship to size and iron content. *Atmospheric Chemistry and Physics*, *19*(24), 15503–15531. <https://doi.org/10.5194/acp-19-15503-2019>
- Dietl, C., Reifenhäuser, W., & Peichl, L. (1997). Association of antimony with traffic — Occurrence in airborne dust, deposition, and accumulation in standardized grass cultures. *Science of the Total Environment*, *205*(2–3), 235–244. [https://doi.org/10.1016/S0048-9697\(97\)00204-0](https://doi.org/10.1016/S0048-9697(97)00204-0)
- Di Mauro, B., Garzonio, R., Rossini, M., Filippa, G., Pogliotti, P., Galvagno, M., et al. (2019). Saharan dust events in the European Alps: Role in snowmelt and geochemical characterization. *The Cryosphere*, *13*(4), 1147–1165. <https://doi.org/10.5194/tc-13-1147-2019>
- Doherty, S. J., Grenfell, T. C., Forsstrom, S., Hegg, D. L., Brandt, R. E., & Warren, S. G. (2013). Observed vertical redistribution of black carbon and other insoluble light-absorbing particles in melting snow. *Journal of Geophysical Research: Atmospheres*, *118*(11), 5553–5569. <https://doi.org/10.1002/jgrd.50235>
- Dris, R., Gasperi, J., Saad, M., Mirande, C., & Tassin, B. (2016). Synthetic fibers in atmospheric fallout: A source of microplastics in the environment? *Marine Pollution Bulletin*, *104*(1–2), 290–293. <https://doi.org/10.1016/j.marpolbul.2016.01.006>
- Dumont, M., Tuzet, F., Gascoin, S., Picard, G., Kutuzov, S., Lafaysse, M., et al. (2020). Accelerated snow melt in the Russian Caucasus mountains after the Saharan dust outbreak in March 2018. *Journal of Geophysical Research: Earth Surface*, *125*(9). <https://doi.org/10.1029/2020JF005641>

- Duniway, M. C., Pfennigwerth, A., Fick, S. E., Nauman, T. W., Belnap, J., & Barger, N. N. (2019). Wind erosion and dust from US drylands: A review of causes, consequences, and solutions in a changing world. *Ecosphere*, *10*(3), e02650. <https://doi.org/10.1002/ecs2.2650>
- Engelbrecht, J. P., Moosmüller, H., Pincock, S., Jayanty, R. K. M., Lersch, T., & Casuccio, G. (2016). Technical note: Mineralogical, chemical, morphological, and optical interrelationships of mineral dust re-suspensions. *Atmospheric Chemistry and Physics*, *16*(17), 10809–10830. <https://doi.org/10.5194/acp-16-10809-2016>
- EPA (U.S. Environmental Protection Agency). (1996). Study of Hazardous air pollutant emissions from electric utility steam generating units. *Interim final report*. EPA-453/R-96-013a.
- Evangelou, N., Grythe, H., Klimont, Z., Heyes, C., Eckhardt, S., Lopez-Aparicio, S., & Stohl, A. (2020). Atmospheric transport is a major pathway of microplastics to remote regions. *Nature Communications*, *11*(1), 3381. <https://doi.org/10.1038/s41467-020-17201-9>
- Fairlie, T. D., Jacob, D. J., & Park, R. J. (2007). The impact of transpacific transport of mineral dust in the United States. *Atmospheric Environment*, *41*(6), 1251–1266. <https://doi.org/10.1016/j.atmosenv.2006.09.048>
- Finkelman, R. B., Orem, W., Castranova, V., Tatu, C. A., Belkin, H. E., Zheng, B., et al. (2002). Health impacts of coal and coal use: Possible solutions. *International Journal of Coal Geology*, *50*(1–4), 425–443. [https://doi.org/10.1016/s0166-5162\(02\)00125-8](https://doi.org/10.1016/s0166-5162(02)00125-8)
- Fischer, E. V., Hsu, N. C., Jaffe, D. A., Jeong, M.-J., & Gong, S. L. (2009). A decade of dust: Asian dust and springtime aerosol load in the U.S. Pacific Northwest. *Geophysical Research Letters*, *36*(3), L03821. <https://doi.org/10.1029/2008GL036467>
- Flanner, M. G., Liu, X., Zhou, C., Penner, J. E., & Jiao, C. (2012). Enhanced solar energy absorption by internally-mixed black carbon in snow grains. *Atmospheric Chemistry and Physics*, *12*(10), 4699–4721. <https://doi.org/10.5194/acp-12-4699>
- Flanner, M. G., Zender, C. S., Hess, P. G., Mahowald, N. M., Painter, T. H., Ramanathan, V., & Rasch, P. J. (2009). Springtime warming and reduced snow cover from carbonaceous particles. *Atmospheric Chemistry and Physics*, *9*(7), 2481–2497. <https://doi.org/10.5194/acp-9-2481-2009>
- Flanner, M. G., Zender, C. S., Randerson, J. T., & Rasch, P. J. (2007). Present-day climate forcing and response from black carbon in snow. *Journal of Geophysical Research*, *112*(D11), D11202. <https://doi.org/10.1029/2006JD008003>
- Ghio, A. J., Kummarapurugu, S. T., Tong, H., Soukup, J. M., Dailey, L. A., Boykin, E., et al. (2014). Biological effects of desert dust in respiratory epithelial cells and a murine model. *Inhalation Toxicology*, *26*(5), 299–309. <https://doi.org/10.3109/08958378.2014.8881>
- Gleason, K. E., McConnell, J. R., Arienzo, M. M., Sexstone, G. A., & Rahimi, S. (2022). Black carbon dominated dust in recent radiative forcing on Rocky Mountain snowpacks. *Environmental Research Letters*, *17*(5), 054045. <https://doi.org/10.1088/1748-9326/ac681b>
- Go, S., Lyapustin, A., Schuster, G. L., Choi, M., Ginoux, P., Chin, M., et al. (2021). Inferring iron oxides species content in atmospheric mineral dust from DSCOVR EPIC observations. *Atmospheric Chemistry and Physics Discussions*. <https://doi.org/10.5194/acp-2021-599>
- Goddard, S. L., Williams, K. R., Robins, C., & Brown, R. J. C. (2019). Determination of antimony and barium in UK air quality samples as indicators of non-exhaust traffic emissions. *Environmental Monitoring and Assessment*, *191*(641), 641. <https://doi.org/10.1007/s10661-019-7774-8>
- Goldstein, H. L., Reynolds, R. L., Molden, N., Lowers, H., Breit, G. N., Williams, E. W., et al. (2024). Physical and chemical data for dust deposited on Colorado Rocky Mountain snow cover during water year 2013 through water year 2016 [Dataset]. *U.S. Geological Survey data release*. <https://doi.org/10.5066/P13HIOO8>
- Gonet, T., & Maher, B. A. (2019). Airborne, vehicle-derived Fe-bearing nanoparticles in the urban environment: A review. *Environmental Science and Technology*, *53*(17), 9970–9991. <https://doi.org/10.1021/acs.est.9b01505>
- Gonet, T., Maher, B. A., Nyirő-Kósa, I., Pósfai, M., Vaculík, M., & Kukutschová, J. (2021). Size-resolved, quantitative evaluation of the magnetic mineralogy of airborne brake-wear particulate emissions. *Environmental Pollution*, *288*, 117808. <https://doi.org/10.1016/j.envpol.2021.117808>
- Goodman, M. M., Carling, G. T., Fernandez, D. P., Rey, K. A., Hale, C. A., Bickmore, B. R., et al. (2019). Trace element chemistry of atmospheric deposition along the Wasatch Front (Utah, USA) reflects regional playa dust and local urban aerosols. *Chemical Geology*, *530*, 119317. 0009-2541. <https://doi.org/10.1016/j.chemgeo.2019.119317>
- Greer, J. B., Dalsky, E. M., Lane, R. F., & Hansen, J. D. (2023). Tire-derived transformation product 6PPD-Quinone induces mortality and transcriptionally disrupts vascular permeability pathways in developing coho salmon. *Environmental Science and Technology*, *57*(30), 10940–10950. <https://doi.org/10.1021/acs.est.3c01040>
- Grigoratos, T., & Martini, G. (2015). Brake wear particle emissions: A review. *Environmental Science and Pollution Research*, *22*(4), 2491–2504. <https://doi.org/10.1007/s11356-014-3696-8>
- Hadley, O. L., Corrigan, C. E., Kirchstetter, T. W., Cliff, S. S., & Ramanathan, V. (2010). Measured black carbon deposition on the Sierra Nevada snowpack and implication for snowpack retreat. *Atmospheric Chemistry and Physics*, *10*(15), 7505–7513. <https://doi.org/10.5194/acpd-10-7505-2010>
- Hahnenberger, M., & Nicoll, K. (2012). Meteorological characteristics of dust transport events in the Eastern Great Basin of Utah, USA. *Atmospheric Environment*, *60*, 601–612. <https://doi.org/10.1016/j.atmosenv.2012.06.029>
- Hahnenberger, M., & Nicoll, K. (2014). Geomorphic and land cover identification of dust sources in the eastern Great Basin of Utah, U.S.A. *Geomorphology*, *204*, 657–672. <https://doi.org/10.1016/j.geomorph.2013.09.013>
- Hand, J. L., Gill, T. E., & Schichtel, B. A. (2017). Spatial and seasonal variability in fine mineral dust and coarse aerosol mass at remote sites across the United States. *Journal of Geophysical Research: Atmospheres*, *122*(5), 3080–3097. <https://doi.org/10.1002/2016JD026290>
- Hand, J. L., Schichtel, B. A., Pitchford, M., Malm, W. C., & Frank, N. H. (2012). Seasonal composition of remote and urban fine particulate matter in the United States. *Journal of Geophysical Research*, *117*(D5), D05209. <https://doi.org/10.1029/2011JD017122>
- Hand, J. L., White, W. H., Gebhart, K. A., Hyslop, N. P., Gill, T. E., & Schichtel, B. A. (2016). Earlier onset of the spring fine dust season in the southwestern United States. *Geophysical Research Letters*, *43*(8), 4001–4009. <https://doi.org/10.1002/2016GL068519>
- Hao, P. T., Ismail, H., & Hashim, A. S. (2001). Study of two types of styrene butadiene rubber in tire tread compounds. *Polymer Testing*, *20*(5), 539–544. [https://doi.org/10.1016/S0142-9418\(00\)00073-8](https://doi.org/10.1016/S0142-9418(00)00073-8)
- He, C. (2022). Modelling light-absorbing particle–snow–radiation interactions and impacts on snow albedo: Fundamentals, recent advances and future directions. *Environmental Chemistry*, *19*(5), 296–311. <https://doi.org/10.1071/en22013>
- He, C., Liou, K. N., Takano, Y., Chen, F., & Barlage, M. (2019). Enhanced snow absorption and albedo reduction by dust-snow internal mixing: Modeling and parameterization. *Journal of Advances in Modeling Earth Systems*, *11*(11), 3755–3776. <https://doi.org/10.1029/2019MS001737>
- Heindel, R. C., Putman, A. L., Murphy, S. F., Repert, D. A., & Hinckley, E.-L. S. (2020). Atmospheric dust deposition varies by season and elevation in the Colorado Front Range, USA. *Journal of Geophysical Research: Earth Surface*, *125*(5), e2019JF005436. <https://doi.org/10.1029/2019JF005436>
- Hidalgo-Ruz, V., Gutow, L., Thompson, R. C., & Thiel, M. (2012). Microplastics in the marine environment: A review of the methods used for identification. *Environmental Science and Technology*, *46*(6), 3060–3075. <https://doi.org/10.1021/es2031505>

- Husar, R. B., Tratt, D. M., Schichtel, B. A., Falke, S. R., Li, F., Jaffe, D., et al. (2001). Asian dust events of April 1998. *Journal of Geophysical Research*, 106(D16), 18317–18330. <https://doi.org/10.1048/0227/01/2000JD900788>
- Jensen, A. S., Rittger, K., & Raleigh, M. S. (2024). Spatio-temporal patterns and trends in MODIS-retrieved radiative forcing by snow impurities over the Western US from 2001–2022. *Environmental Research: Climate*, 3(2), 025001. <https://doi.org/10.1088/2752-5295/ad285a>
- Kandakji, T., Gill, T. E., & Lee, J. A. (2020). Identifying and characterizing dust point sources in the southwestern United States using remote sensing and GIS. *Geomorphology*, 353, 107019. <https://doi.org/10.1016/j.geomorph.2019.107019>
- Kaspari, S., Painter, T. H., Gysel, M., Skiles, S. M., & Schwikowski, M. (2014). Seasonal and elevational variations of black carbon and dust in snow and ice in the Solu-Khumbu, Nepal and estimated radiative forcings. *Atmospheric Chemistry and Physics*, 14(15), 8089–8103. <https://doi.org/10.5194/acp-14-8089-2014>
- Kaspari, S., Skiles, S. M., Delaney, I., Dixon, D., & Painter, T. H. (2015). Accelerated glacier melt on Snow Dome, Mount Olympus, Washington, USA, due to deposition of black carbon and mineral dust from wildfire. *Journal of Geophysical Research: Atmospheres*, 120(7), 2793–2807. <https://doi.org/10.1002/2014jd022676>
- Kavouras, I. G., Etyemezian, V., Xu, J., DuBois, D. W., Green, M., & Pitchford, M. (2009). Assessment of the local windblown component of dust in the western United States. *Journal of Geophysical Research*, 112(D8), D08211. <https://doi.org/10.1029/2006JD007832>
- Kokaly, R. F. (2011). PRISM—processing routines in IDL for spectroscopic measurements (installation manual and user's guide, version 1.0). U. S. Geological Survey Open-File Report 2011–1155 (p. 431). Retrieved from <http://pubs.usgs.gov/of/2011/1155/>
- Kokaly, R. F., Clark, R. N., Swayze, G. A., Livo, K. E., Hoefen, T. M., Pearson, N. C., et al. (2017). *USGS spectral library version 7 data: U.S. Geological Survey data release* (Vol. 61). United States Geological Survey (USGS). <https://doi.org/10.3133/ds1035>
- Kokaly, R. F., & Skidmore, A. K. (2015). Plant phenolics and absorption features in vegetation reflectance spectra near 1.66 μm . *International Journal of Applied Earth Observation and Geoinformation*, 43, 55–83. <https://doi.org/10.1016/j.jag.2015.01.010>
- Kole, P. J., Löhr, A. J., Van Belleghem, F. G., & Ragas, A. M. (2017). Wear and tear of tyres: A stealthy source of microplastics in the environment. *International Journal of Environmental Research and Public Health*, 14(10), 1265. <https://doi.org/10.3390/ijerph14101265>
- Lafon, S., Rajot, J. L., Alfaro, S. C., & Gaudichet, A. (2004). Assessing the iron-oxides content in desert aerosols. *Atmospheric Environment*, 38(8), 1211–1218. <https://doi.org/10.1016/j.atmosenv.2003.11.006>
- Lafon, S., Sokolik, I. N., Rajot, J. L., Caquineau, S., & Gaudichet, A. (2006). Characterization of iron oxides in mineral dust aerosols: Implications for light absorption. *Journal of Geophysical Research*, 111(D21207). <https://doi.org/10.1029/2005JD007016>
- Landry, C. C., Buck, K., Raleigh, M. S., & Clark, M. P. (2014). Mountain system monitoring at Senator Beck Basin, San Juan Mountains, Colorado: A new integrative data source to develop and evaluate models snow and hydrologic processes. *Water Resources Research*, 50(2), 1773–1788. <https://doi.org/10.1002/2013WR013711>
- Lawrence, C. R., Painter, T. H., Landry, C. C., & Neff, J. C. (2010). Contemporary geochemical composition and flux of aeolian dust to the San Juan Mountains, Colorado, United States. *Journal of Geophysical Research*, 115(G03007). <https://doi.org/10.1029/2009JG001077>
- Lawrence, C. R., Reynolds, R. L., Ketterer, M., & Neff, J. C. (2013). Aeolian controls on soil geochemistry and weathering fluxes in high-elevation ecosystems of the Rocky Mountains, USA. *Geochimica et Cosmochimica Acta*, 107, 27–46. <https://doi.org/10.1016/j.gca.2012.12.023>
- Li, J., Okin, G. S., Skiles, S. M., & Painter, T. H. (2013). Relating variation of dust on snow to bare soil dynamics in the western United States. *Environmental Research Letters*, 8(4), 044054. <https://doi.org/10.1088/1748-9326/8/4/044054>
- Lough, G. C., Schauer, J. J., Park, J., Shafer, M. M., Deminter, J. T., & Weinstein, J. P. (2005). Emissions of metals associated with motor vehicle roadways. *Environmental Science and Technology*, 39(3), 826–836. <https://doi.org/10.1021/es048715f>
- Mangum, A. L., Carling, G. T., Bickmore, B. R., Webb, N., Leifi, D. L., Brahney, J., et al. (2024). Characterizing variability in geochemistry and mineralogy of western US dust sources. *Aeolian Research*, 70, 100941. <https://doi.org/10.1016/j.aeolia.2024.100941>
- Miller, M. E., Bowker, M. A., Reynolds, R. L., & Goldstein, H. L. (2012). Post-fire land treatments and wind erosion - Lessons from the Milford Flat Fire, UT, USA. *Aeolian Research*, 7, 29–44. <https://doi.org/10.1016/j.aeolia.2012.04.001>
- Ming, J., & Wang, F. (2021). Microplastics' hidden contribution to snow melting. *Eos*, 102. <https://doi.org/10.1029/2021EO155631>
- Moosmüller, H., Engelbrecht, J. P., Skiba, M., Frey, G., Chakrabarty, R. K., & Arnott, W. P. (2012). Single scattering albedo of fine mineral dust aerosols controlled by iron concentration. *Journal of Geophysical Research*, 117(D11), D11210. <https://doi.org/10.1029/2011JD01690>
- Moskowitz, B. M., Reynolds, R. L., Goldstein, H. L., Berquó, T. S., Kokaly, R. F., & Bristow, C. S. (2016). Iron oxide minerals in dust-source sediments from the Bodélé Depression, Chad. Implications for radiative properties and Fe bioavailability of dust plumes from the Sahara. *Aeolian Research*, 22, 93–106. <https://doi.org/10.1016/j.aeolia.2016.07.001>
- Moteki, N., Adachi, K., Ohata, S., Yoshida, A., Harigaya, T., Koike, M., & Kondo, Y. (2017). Anthropogenic iron oxide aerosols enhance atmospheric heating. *Nature Communications*, 8(1), 1–11. <https://doi.org/10.1038/ncomms15329>
- Munroe, J. S. (2014). Properties of modern dust accumulating in the Uinta Mountains, Utah, USA, and implications for the regional dust system of the Rocky Mountains. *Earth Surface Processes and Landforms*, 39(14), 1979–1988. <https://doi.org/10.1002/esp.3608>
- Munroe, J. S., Norris, E. D., Carling, G. T., Beard, B. L., Satkoski, A. M., & Liu, L. (2019). Isotope fingerprinting reveals western North American sources of modern dust in the Uinta Mountains, Utah, USA. *Aeolian Research*, 38, 39–47. <https://doi.org/10.1016/j.aeolia.2019.03.005>
- Munroe, J. S., Soderstrom, E. J., Klutmeier, C. L., Tappa, M. J., Mallia, D. V., & Bauer, A. M. (2023). Regional sources control dust in the mountain critical zone of the Great Basin and Rocky Mountains, USA. *Environmental Research Letters*, 18(10), 104034. <https://doi.org/10.1088/1748-9326/acfb26>
- Munson, S. M., Belnap, J., & Okin, G. S. (2011). Responses of wind erosion to climate-induced vegetation changes on the Colorado Plateau. *Proceedings of the National Academy of Sciences USA*, 108(10), 3854–3859. <https://doi.org/10.1073/pnas.1014947108>
- Nagorski, S. A., Kaspari, S. D., Hood, E., Fellman, J. B., & Skiles, S. M. (2019). Radiative forcing by dust and black carbon on the Juneau Icefield, Alaska. *Journal of Geophysical Research: Atmospheres*, 124(7), 3943–3959. <https://doi.org/10.1029/2018JD029411>
- Naple, P., Skiles, S. M., Lang, O. I., Rittger, K., Lenard, S. J. P., Burgess, A., & Painter, T. H. (2024). Dust on snow radiative forcing and contribution to melt in the Colorado River Basin over the MODIS record. *ESS Open Archive*. <https://doi.org/10.22541/essoar.172987451.11953219/v1>
- Nauman, T. W., Duniway, M. C., Webb, N. P., & Belnap, J. (2018). Elevated dust emissions on the Colorado Plateau, USA: The role of grazing, vehicle disturbance, and increasing aridity. *Earth Surface Processes and Landforms*, 43(14), 2897–2914. <https://doi.org/10.1002/esp.4457>
- Nauman, T. W., Munson, S. M., Dhital, S., Webb, N. P., & Duniway, M. C. (2023). Synergistic soil, land use, and climate influences on wind erosion on the Colorado Plateau: Implications for management. *Science of the Total Environment*, 893, 164605. <https://doi.org/10.1016/j.scitotenv.2023.164605>
- Neff, J. C., Reynolds, R. L., Munson, S., Fernandez, D., & Belnap, J. (2013). The role of dust storms in atmospheric particle concentrations at two sites in the western U.S. *Journal of Geophysical Research*, 118(19), 11201–11212. <https://doi.org/10.1002/jgrd.50855>

- Oaida, C. M., Xue, Y., Flanner, M. G., Skiles, S. M., De Sales, F., & Painter, T. H. (2015). Improving snow albedo processes in WRF/SSiB regional climate model to assess impact of dust and black carbon in snow on surface energy balance and hydrology over western U.S. *Journal of Geophysical Research: Atmospheres*, *120*(8), 3228–3248. <https://doi.org/10.1002/2014JD022444>
- Olmez, I., & Gordon, G. E. (1985). Rare earths: Atmospheric signatures for oil-fired power plants and refineries. *Science*, *229*(4717), 966–968. <https://doi.org/10.1126/science.229.4717.966>
- O'Loughlin, D. P., Haugen, M. J., Day, J., Brown, A. S., Braysher, E. C., Molden, N., et al. (2023). Multi-element Analysis of Tyre Rubber for Metal Tracers. *Environment International*, *108047*.
- Painter, T. H., Barrett, A. P., Landry, C. C., Neff, J. C., Cassidy, M. P., Lawrence, C. R., et al. (2007). Impact of disturbed desert soils on duration of mountain snow cover. *Geophysical Research Letters*, *34*(12). <https://doi.org/10.1029/2007GL030284>
- Painter, T. H., Bryant, A., & Skiles, S. M. (2012). Radiative forcing by light absorbing impurities in snow from MODIS surface reflectance data. *Geophysical Research Letters*, *39*(17). <https://doi.org/10.1029/2012GL052457>
- Painter, T. H., Deems, J. S., Belnap, J., Hamlet, A. F., Landry, C. C., & Udall, B. (2010). Response of Colorado River runoff to dust radiative forcing in snow. *Proceedings of the National Academy of Sciences USA*, *107*(40), 17125–17130. <https://doi.org/10.1073/pnas.0913139107>
- Painter, T. H., Skiles, S. M., Deems, J., Bryant, A., & Landry, C. C. (2012). Dust radiative forcing in snow of the Upper Colorado River basin: Part I. A 6 year record of energy balance, radiation, and dust concentrations. *Water Resources Research*, *48*(7). <https://doi.org/10.1029/2012WR011985>
- Painter, T. H., Skiles, S. M., Deems, J. S., Brandt, W. T., & Dozier, J. (2018). Variation in rising limb of Colorado River snowmelt runoff hydrograph controlled by dust radiative forcing in snow. *Geophysical Research Letters*, *45*(2), 797–808. <https://doi.org/10.1002/2017GL075826>
- Phillips, M., & Doesken, N. (2011). Continental wind patterns associated with Colorado alpine dust deposition—An application of the BLM/USFS RAWs network. *Journal of Service Climatology*, *5*, 1–11.
- Rahimi, S., Liu, X., Zhao, C., Lu, Z., & Lebo, Z. J. (2020). Examining the atmospheric radiative and snow-darkening effects of black carbon and dust across the Rocky Mountains of the United States using WRF-Chem. *Atmospheric Chemistry and Physics*, *20*(18), 10911–10935. <https://doi.org/10.5194/acp-20-10911-2020>
- Revell, L. E., Kuma, P., Le Ru, E. C., Somerville, W. R., & Gaw, S. (2021). Direct radiative effects of airborne microplastics. *Nature*, *598*(7881), 462–467. <https://doi.org/10.1038/s41586-021-03864-x>
- Reynolds, R. L., Cattle, S. R., Moskowitz, B. M., Goldstein, H. L., Yauk, K., Flagg, C., et al. (2014). Iron oxide minerals in dust of the Red Dawn event in eastern Australia, September 2009. *Aeolian Research*, *15*, 1–13. <https://doi.org/10.1016/j.aeolia.2014.02.003>
- Reynolds, R. L., Goldstein, H. L., Moskowitz, B. M., Bryant, A. C., Skiles, S. M., Kokaly, R. F., et al. (2014). Composition of dust deposited to snow cover in the Wasatch Range (Utah, USA). Controls on radiative properties of snow cover and comparison to some dust-source sediments. *Aeolian Research*, *15*, 73–90. <https://doi.org/10.1016/j.aeolia.2013.08.001>
- Reynolds, R. L., Goldstein, H. L., Moskowitz, B. M., Kokaly, R. F., Munson, S. M., Solheid, P., et al. (2020). Dust deposited on snow cover in the San Juan Mountains, Colorado, 2011–2016: Compositional variability bearing on snow-melt effects. *Journal of Geophysical Research: Atmospheres*, *125*(7), e2019JD032210. <https://doi.org/10.1029/2019JD032210>
- Reynolds, R. L., Molden, N., Kokaly, R. F., Lowers, H., Breit, G. N., Goldstein, H. L., et al. (2024). Microplastic and Associated Black Particles from Road-tire Wear: Implications for Radiative Effects across the Cryosphere and in the Atmosphere. *Journal of Geophysical Research: Atmospheres*, *129*(19), e2024JD041116. <https://doi.org/10.1029/2024JD041116>
- Reynolds, R. L., Mordecai, J., Rosenbaum, J., Ketterer, M. E., Walsh, M. K., & Moser, K. (2010). Compositional changes in sediments of subalpine lakes, Uinta Mountains, Utah: Evidence for the effects of human activity on atmospheric dust inputs. *Journal of Paleolimnology*, *44*(1), 161–175. ISSN 0921-2728. <https://doi.org/10.1007/s10933-009-9394-8>
- Reynolds, R. L., Munson, S. M., Fernandez, D. P., & Neff, J. C. (2016). Concentrations of mineral aerosol from desert to plains across the central Rocky Mountains, western United States. *Aeolian Research*, *23*, 21–35. <https://doi.org/10.1016/j.aeolia.2016.09.001>
- Routson, C. C., Arcusa, S. H., McKay, N. P., & Overpeck, J. T. (2019). A 4,500-year-long record of southern Rocky Mountain dust deposition. *Geophysical Research Letters*, *46*(14), 8281–8288. <https://doi.org/10.1029/2019GL083255>
- Rudnick, R. L., & Gao, S. (2003). Composition of the Continental Crust. In H. D. Holland & K. K. Turekian (Eds.), *Treatise on Geochemistry* 659 pp. ISBN 0-08-043751-6. Elsevier (Vol. 3, pp. 1–64). <https://doi.org/10.1016/B0-08-043751-6/03016-4>
- Sarangi, C., Qian, Y., Rittger, K., Ruby Leung, L., Chand, D., Bormann, K. J., & Painter, T. H. (2020). Dust dominates high-altitude snow darkening and melt over high-mountain Asia. *Nature Climate Change*, *10*(11), 1045–1051. <https://doi.org/10.1038/s41558-020-00909-3>
- Schauer, J. J., Lough, G. C., Shafer, M. M., Christensen, W. F., Arndt, M. F., DeMinter, J. T., & Park, J. S. (2006). Characterization of metals emitted from motor vehicles. *Research Report - Health Effects Institute*, *133*, 1–76. discussion 77–88. PMID: 16669575.
- Scholz, J., & Brahney, J. (2022). Evidence for multiple potential drivers of increased phosphorus in high-elevation lakes. *Science of the Total Environment*, *825*, 153939. <https://doi.org/10.1016/j.scitotenv.2022.153939>
- Senior, C., Granite, E., Linak, W., & Seames, W. (2020). Chemistry of Trace Inorganic Elements in Coal Combustion Systems: A Century of Discovery. *Energy and Fuels*, *34*(12), 15141–15168. <https://doi.org/10.1021/acs.energyfuels.0c02375>
- Skiles, S. M., Flanner, M., Cook, J. M., Dumont, M., & Painter, T. H. (2018). Radiative forcing by light-absorbing particles in snow. *Nature Climate Change*, *8*(11), 964–971. <https://doi.org/10.1038/s41558-018-0296-5>
- Skiles, S. M., & Painter, T. H. (2016). A Nine-Year Record of Dust on Snow in the Colorado River Basin. In B. Chapter & B. E. Ralston (Eds.), *Proceedings of the 12th biennial conference of research on the Colorado plateau* (p. 11). U.S. Geological Survey Scientific Investigations Report 2015–5180. <https://doi.org/10.3133/sir20155180>
- Skiles, S. M., & Painter, T. H. (2017). Daily evolution in dust and black carbon content, snow grain size, and snow albedo during snowmelt, Rocky Mountains, Colorado. *Journal of Glaciology*, *63*(237), 118–132. <https://doi.org/10.1017/jog.2016.125>
- Skiles, S. M., & Painter, T. H. (2018). Assessment of radiative forcing by light-absorbing particles in snow from in-situ observations with radiative transfer modeling. *Journal of Hydrometeorology*, *19*(8), 1397–1409. <https://doi.org/10.1175/JHM-D-18-0072.1>
- Skiles, S. M., Painter, T. H., Belnap, J., Holland, L., Reynolds, R. L., Goldstein, H. L., & Lin, J. (2015). Regional variability in dust-on-snow processes and impacts in the Upper Colorado River Basin. *Hydrological Processes*, *29*(26), 5397–5413. <https://doi.org/10.1002/hyp.10569>
- Skiles, S. M., Painter, T. H., Deems, J., Landry, C., & Bryant, A. (2012). Dust radiative forcing in snow of the Upper Colorado River basin: Part II. Interannual variability in radiative forcing and snowmelt rates. *Water Resources Research*, *48*(7). <https://doi.org/10.1029/2012WR011986>
- Skiles, S. M., Painter, T. H., & Okin, G. S. (2017). A method to retrieve the spectral complex refractive index and single scattering optical properties of dust deposited in mountain snow. *Journal of Glaciology*, *63*(237), 133–147. <https://doi.org/10.1017/jog.2016.126>
- Sokolik, I. N., Winker, D. M., Bergametti, G., Gillette, D. A., Carmichael, G., Kaufman, Y. J., et al. (2001). Introduction to special section: Outstanding problems in quantifying the radiative impacts of mineral dust. *Journal of Geophysical Research*, *106*(D16), 18015–18027. <https://doi.org/10.1029/2000jd900498>

- Sommer, F., Dietze, V., Baum, A., Sauer, J., Gilge, S., Maschowski, C., & Gieré, R. (2018). Tire abrasion as a major source of microplastics in the environment. *Aerosol and Air Quality Research*, 18(8), 2014–2028. <https://doi.org/10.4209/aaqr.2018.03.0099>
- Steltzer, H., Landry, C., Painter, T. H., Anderson, J., & Ayres, E. (2009). Biological consequences of earlier snowmelt from desert dust deposition in alpine landscapes. *Proceedings of the National Academy of Sciences, USA*, 106(28), 11629–11634. <https://doi.org/10.1073/pnas.0900758106>
- Tian, Z., Zhao, H., Peter, K. T., Gonzalez, M., Wetzel, J., Wu, C., et al. (2021). A ubiquitous tire rubber-derived chemical induces acute mortality in coho salmon. *Science*, 371(6525), 185–189. <https://doi.org/10.1126/science.abd6951>
- Trainic, M., Flores, J. M., Pinkas, I., Pedrotti, M. L., Lombard, F., Bourdin, G., et al. (2020). Airborne microplastic particles detected in the remote marine atmosphere. *Communications Earth Environment*, 1, 64. <https://doi.org/10.1038/s43247-020-00061-y>
- Turley, C. D., Brencley, D. L., & Landolt, R. R. (1973). Barium additives as diesel smoke suppressants. *Journal of the Air Pollution Control Association*, 23(9), 783–787. <https://doi.org/10.1080/00022470.1973.10469844>
- Tyree, G. L., Chappell, A., Villarreal, M. L., Dhital, S., Duniway, M. C., Edwards, B. L., et al. (2024). Oil and gas development influences potential for dust emission from the Upper Colorado River Basin, USA. *Earth Surface Processes and Landforms*, 49(11), 3292–3307. <https://doi.org/10.1002/esp.5887>
- Udall, B. (2013). Water: Impacts, Risks, and Adaptation. In G. Garfin, A. Jardine, R. Merideth, M. Black, & S. LeRoy (Eds.), *Assessment of climate change in the southwest United States: A report prepared for the national climate assessment, A report by the southwest climate alliance* (pp. 197–217). Island Press.
- VanCuren, R. A., & Cahill, T. A. (2002). Asian aerosols in North America: Frequency and concentration of fine dust. *Journal of Geophysical Research*, 107(D24), 4804. <https://doi.org/10.1029/2002JD002204>
- Van Metre, P. C., Mahler, B. J., & Wilson, J. T. (2009). PAHs underfoot: Contaminated dust from coal-tar seal-coated pavement is widespread in the United States. *Environmental Science and Technology*, 43(1), 20–25. <https://doi.org/10.1021/es802119h>
- Viviroli, D., Dürr, H. H., Messerli, B., Meybeck, M., & Weingartner, R. (2007). Mountains of the world, water towers for humanity: Typology, mapping, and global significance. *Water Resources Research*, 43(7). <https://doi.org/10.1029/2006WR005653>
- Vogelsang, C., Lusher, A. L., Dadkhah, M. E., Sundvor, I., Umar, M., Rannekleiv, S. B., et al. (2020). Microplastics in road dust—Characteristics, pathways and measures. <https://www.miljodirektoratet.no/globalassets/publikasjoner/M959/M959.pdf>
- Wagner, S., Hüffer, T., Klöckner, P., Wehrhahn, M., Hofmann, T., & Reemtsma, T. (2018). Tire wear particles in the aquatic environment—a review on generation, analysis, occurrence, fate and effects. *Water Research*, 139, 83–100. <https://doi.org/10.1016/j.watres.2018.03.051>
- Wang, X., Doherty, S. J., & Huang, J. P. (2013). Black carbon and other light-absorbing impurities in snow across Northern China. *Journal of Geophysical Research: Atmospheres*, 118(3), 1471–1492. <https://doi.org/10.1029/2012jd018291>
- Wetherbee, G. A., Baldwin, A. K., & Ranville, J. F. (2019). It is raining plastic. *U.S. Geological Survey Open-file Report 2019-1048*, 1 plate. <https://doi.org/10.3133/ofr20191048>
- Wolf, R. E., & Adams, M. (2015). Multi-elemental analysis of aqueous geochemical samples by quadrupole inductively coupled plasma-mass spectrometry (ICP-MS). U.S. Geological Survey Open-File Report 2015-1010. <https://doi.org/10.3133/ofr20151010>
- Wu, C., Liu, X., Lin, Z., Rahimi-Esfarjani, S. R., & Zheng Lu, Z. (2018). Impacts of absorbing aerosol deposition on snowpack and hydrologic cycle in the Rocky Mountain region based on variable-resolution CESM (VR-CESM) simulations. *Atmospheric Chemistry and Physics*, 18(2), 511–533. <https://doi.org/10.5194/acp-18-511-2018>
- Xiao, S., Cui, Y., Brahney, J., Mahowald, N. M., & Li, Q. (2023). Long-distance atmospheric transport of microplastic fibres influenced by their shapes. *Nature Geoscience*, 16(10), 863–870. <https://doi.org/10.1038/s41561-023-01264-6>
- Yang, C., Niu, S., Xia, Y., & Wu, J. (2023). Microplastics in urban road dust: Sampling, analysis, characterization, pollution level, and influencing factors. *TrAC, Trends in Analytical Chemistry*, 168, 117348. <https://doi.org/10.1016/j.trac.2023.117348>
- Yasunari, T. J., Koster, R. D., Lau, W. K. M., & Kim, K. M. (2014). Impact of snow darkening via dust, black carbon, and organic carbon on boreal spring climate in the Earth system. *Journal of Geophysical Research: Atmospheres*, 120(11), 5485–5503. <https://doi.org/10.1002/2014jd022977>
- Zambrano, M. C., Pawlak, J. J., Daystar, J., Ankeny, M., Cheng, J. J., & Venditti, R. A. (2019). Microfibers generated from the laundering of cotton, rayon and polyester based fabrics and their aquatic biodegradation. *Marine Pollution Bulletin*, 142, 394–407. <https://doi.org/10.1016/j.marpolbul.2019.02.062>
- Zhang, X., Zhao, L., Tong, D., Wu, G., Dan, M., & Teng, B. (2016). A systematic review of global desert dust and associated human health effects. *Atmosphere*, 7(12), 158. <https://doi.org/10.3390/atmos7120158>
- Zhang, X. L., Wu, G. J., Zhang, C. L., Xu, T. L., & Zhou, Q. Q. (2015). What's the real role of iron-oxides in the optical properties of dust aerosols? *Atmospheric Chemistry and Physics*, 15(4), 5619–5662. <https://doi.org/10.5194/acpd-15-12159-2015>
- Zhang, Y., Gao, T., Kang, S., & Sillanpää, M. (2019). Importance of atmospheric transport for microplastics deposited in remote areas. *Environmental Pollution*, 254, 112953. <https://doi.org/10.1016/j.envpol.2019.07.121>
- Zhang, Y. L., Kang, S., Sprenger, M., Cong, Z., Gao, T., Li, C., et al. (2018). Black carbon and mineral dust in snow cover on the Tibetan Plateau. *The Cryosphere*, 12(2), 413–431. <https://doi.org/10.5194/tc-12-413-2018>
- Zhang, Z., Goldstein, H. L., Reynolds, R. L., Hu, Y., Wang, X., & Zhu, M. (2018). Phosphorus speciation and solubility in aeolian dust deposited in the interior American West. *Environmental Science and Technology*, 52(5), 2658–2667. <https://doi.org/10.1021/acs.est.7b04729>
- Zhao, C., Hu, Z., Qian, Y., Leung, L., Huang, J., Huang, M., et al. (2014). Simulating black carbon and dust and their radiative forcing in seasonal snow: A case study over North China with field campaign measurements. *Atmospheric Chemistry and Physics*, 14(20), 11475–11491. <https://doi.org/10.5194/acp-14-11475-2014>
- Zhao, T. L., Gong, S. L., Zhang, X. Y., & Jaffe, D. A. (2008). Asian dust storm influence on North American ambient PM levels: Observational evidence and controlling factors. *Atmospheric Chemistry and Physics*, 8(10), 2717–2728. <https://doi.org/10.5194/acp-8-2717-2008>
- Zhong, X., Kang, S., Zhang, W., Yang, J., Niu, H., Liu, Y., et al. (2021). Continuously observed light absorbing impurities in snow cover over the southern Altai Mts. in China: Concentrations, impacts and potential sources. *Environmental Pollution*, 270, 116234. <https://doi.org/10.1016/j.envpol.2020.116234>
- Zimmermann, F., Weinbruch, S., Schutz, L., Hofmann, H., Ebert, M., Kandler, K., & Worringer, A. (2008). Ice nucleation properties of the most abundant mineral dust phases. *Journal of Geophysical Research*, 113(D23), D23204. <https://doi.org/10.1029/2008JD010655>